NASA TN D-183

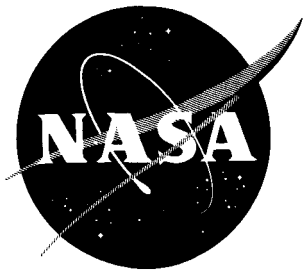

TECHNICAL NOTE
D-183

EFFECTS OF A LOWER SURFACE JET ON THE LIFT-DRAG RATIO OF A 45° SWEPTBACK WING AT A MACH NUMBER OF 2.01

By Emma Jean Landrum

Langley Research Center
Langley Field, Va.

NATIONAL AERONAUTICS AND SPACE ADMINISTRATION

WASHINGTON

March 1960

NATIONAL AERONAUTICS AND SPACE ADMINISTRATION

TECHNICAL NOTE D-183

EFFECTS OF A LOWER SURFACE JET ON THE LIFT-DRAG RATIO OF A 45° SWEPTBACK WING AT A MACH NUMBER OF 2.01

By Emma Jean Landrum

SUMMARY

An investigation has been conducted in the Langley 4- by 4-foot supersonic pressure tunnel to determine the effects of jet interference on the lift-drag ratio of a wing having 45° sweepback of the quarter-chord line, an aspect ratio of 3.5, a taper ratio of 0.3, and NACA 65A005 airfoil sections parallel to the airstream. The jet was located along the 67-percent-chord station of the lower surface of the wing. Tests were made at angles of attack from -2° to 7° for various jet-deflection angles and momentum coefficients. The Mach number for the investigation was 2.01.

The results indicate some improvement in lift-drag ratios at and near the maximum lift-drag ratio, with decreasing effectiveness as the jet is inclined rearward. The improvement in maximum lift-drag ratio does not appear to be large enough to be of practical use on an actual airplane because of the problems arising from trying to use engine exhaust or engine bypass air as a source of air for the jet.

INTRODUCTION

One of the problems confronting designers of supersonic airplanes is that of improving lift-drag ratio. Recently, interest has been shown in the use of a jet spanning the lower surface of a wing as a method of improving lift-drag ratio by generating favorable interference effects.

Analysis of data obtained at negative angles of attack during an investigation of the aerodynamic characteristics of a jet spoiler (ref. 1) indicated that a lower surface jet might provide some improvement in lift-drag ratio.

The purpose of this report is to present the results of an investigation conducted in the Langley 4- by 4-foot supersonic pressure tunnel to determine the effects of jet-deflection angle and momentum coefficient

on the lift-drag ratio of a wing having a jet located along the lower surface. A semispan-wing model with 45° sweepback of the quarter-chord line tested in the presence of a half-fuselage at angles of attack from -2° to 7° was used for this investigation. The investigation was conducted at a Mach number of 2.01 for Reynolds numbers of 1.5×10^6 and 2.8×10^6 based on the wing mean aerodynamic chord of 10.65 inches.

SYMBOLS

b	wing span, in.
b_j	span of jet, in.
C_D	semispan-wing drag coefficient, Drag/qS
C_L	semispan-wing lift coefficient, Lift/qS
C_l	semispan-wing rolling-moment coefficient, Rolling moment/2qSb
C_m	semispan-wing pitching-moment coefficient referred to $0.25\bar{c}$, Pitching moment/qS$\bar{c}$
C_μ	momentum coefficient (based on semispan-wing area), wV_j/gqS
c	wing local chord, in.
$\bar{c}$	wing mean aerodynamic chord, in.
g	acceleration due to gravity, ft/sec^2
L/D	lift-drag ratio
q	stream dynamic pressure, lb/sq ft
R	Reynolds number, based on mean aerodynamic chord
S	semispan-wing area, sq ft
V_j	jet velocity associated with isentropic expansion to the critical pressure ratio at the jet exit, ft/sec
w	weight-flow rate of air used in jet, lb/sec
y_i	perpendicular distance from plane of symmetry to inboard end of jet, in.

y_o	perpendicular distance from plane of symmetry to outboard end of jet, in.
α	wing angle of attack, deg
Δ	prefix indicating increment due to jet
δ_j	streamwise angle between center line of jet slots and wing surface (see fig. 1), deg

Subscripts:

e	effective, refers to wing coefficients with jet reaction subtracted
max	maximum

APPARATUS

Wind Tunnel

Tests were conducted in the Langley 4- by 4-foot supersonic pressure tunnel which is a rectangular, closed-throat, single-return-type wind tunnel. The flexible nozzle walls were adjusted to give the desired test-section Mach number of 2.01. The dewpoint was kept below -20° F during the tests so that condensation effects were negligible.

Model

The model used in this investigation consisted of a semispan wing and a half-fuselage as shown in figure 1. The wing was made of steel and had 45° sweepback of the quarter-chord line, an aspect ratio of 3.5, a taper ratio of 0.3, and NACA 65A005 airfoil sections parallel to the airstream. A plenum chamber was constructed by milling out a portion of the lower surface of the wing from the wing root to about the 80-percent-semispan station. Interchangeable cover plates were then constructed, each having slots located along the 67-percent-chord station of the wing. The slots were cut at angles of 110°, 130°, and 150° to the surface measured in the streamwise direction (fig. 1). The cover plates for the angles of 110° (configuration 1) and 130° (configuration 2) had 10 slots 1 inch by 0.050 inch at 1/4-inch spacings. There were nine slots 1 inch by 0.054 inch at 3/8-inch spacings in the cover plate for the jet-deflection angle of 150° (configuration 3). In addition to the three basic configurations (configurations 1 to 3) there were two modifications (configurations 4 and 5) to configuration 2. These modifications were

made by reducing the number of slots from 10 to 7, first by sealing the three most inboard slots (configuration 4), and then by sealing the three most outboard slots (configuration 5). Geometrical details of the configurations investigated are given in table I.

The fuselage was constructed of aluminum alloy and had an ogival nose with a fineness ratio of 2.5, a cylindrical center portion, and a boattailed afterbody with a base diameter that was 50 percent of the body maximum diameter (fig. 1).

The wing was mounted on a four-component strain-gage balance which was located in the turntable of a boundary-layer bypass plate installed vertically about 10 inches from the tunnel sidewall. The half-fuselage was mounted on the turntable independently of the wing with 0.030-inch clearance between the wing and fuselage. Angle of attack was changed manually by rotating the turntable on which the model was mounted and was measured by a vernier scale outside the tunnel.

High-pressure air from a dry-air supply outside the tunnel was delivered to the plenum chamber in the wing by a 1-inch-diameter feeder tube about 24 inches long. This tube, which was shielded from the airstream between the bypass plate and the tunnel wall by a fairing, was floated on "O" rings at either end so that the forces transmitted around the balance would be negligible. A valve in the high-pressure air line ahead of the feeder tube was used to control the air supply to the plenum chamber from zero to a maximum of 40 lb/sq in. abs.

TESTS AND TEST PROCEDURES

Wing lift, drag, pitching-moment, and rolling-moment coefficients were measured at various momentum coefficients for each configuration through an angle-of-attack range from -2° to 7°.

The jet-exit area was designed to be small enough to maintain choked flow through the slots at all conditions and thus simplify the determination of the jet-reaction coefficients. The variation of the jet-reaction coefficients with momentum coefficient for each configuration was obtained from tunnel-off calibrations.

Each configuration was tested at a tunnel stagnation pressure of 11.5 lb/sq in. abs, corresponding to a Reynolds number of 2.8×10^6 based on the wing mean aerodynamic chord. Configuration 2 ($\delta_j = 130^{\circ}$) was also tested at a tunnel stagnation pressure of 6 lb/sq in. abs corresponding to a Reynolds number of 1.5×10^6 based on the wing mean aerodynamic chord.

PRECISION OF DATA

The mean Mach number in the region occupied by the model was estimated from calibrations to be 2.01 with local variations smaller than ±0.02. There was no evidence of significant flow angularity.

The angle of attack of the wing root could be set within ±0.05°. The estimated accuracies of the coefficients are as follows:

C_L	±0.003
C_D	±0.0003
C_m	±0.0005
C_l	±0.0006
C_μ	±0.0007

Although the accuracy of the incremental forces is not known, it is believed to be sufficient to indicate the trends of the data. Repeat tests of some of the configurations resulted in nearly identical results. Furthermore, tests of very similar jets on the same model with a different balance indicated excellent agreement.

RESULTS AND DISCUSSION

Basic Wing Characteristics

The variation of wing lift, drag, pitching-moment, and rolling-moment coefficients with angle of attack with the jet inoperative is presented in figure 2. Since the differences in the coefficients for the various configurations tested were small, data are shown for only three configurations.

The basic plots of wing lift, drag, pitching-moment, and rolling-moment coefficients obtained with the jet operating are presented, respectively, in figures 3 to 6. The coefficients are plotted against momentum coefficient for constant angle-of-attack conditions. In general, the effect of increasing the momentum coefficient was to increase the lift and to decrease the drag, pitching moment, and rolling moment. These changes with momentum coefficient were approximately linear. The angle of attack had little effect on the slope of the curves except for drag. For drag coefficient, the slope of the curves with respect to momentum coefficient decreased with increasing angle of attack.

Figure 7 indicates for two of the configurations tested that increasing momentum coefficient decreased C_L for $C_m = 0$ slightly

but had no effect on the slope of the curve of pitching moment with respect to lift coefficient. Similar effects occurred for all the other configurations, although there were small changes in the magnitude of C_L for $C_m = 0$. The data in figure 7 are for the jet-inoperative condition and for the highest momentum coefficient obtained at a Reynolds number of 2.8×10^6 based on the mean aerodynamic chord. Curves for intermediate values of C_μ fell between the curves shown. Configuration 2 was also tested at a Reynolds number of 1.5×10^6 based on the mean aerodynamic chord. For this test condition the maximum value of C_μ was increased from 0.0196 to 0.0376 and the value of C_L for $C_m = 0$ changed from approximately -0.025 to -0.038 which was about a 50-percent change in lift coefficient for a twofold change in momentum coefficient.

Jet Effects on Lift-Drag Ratio

The effectiveness of the jet in producing changes in lift-drag ratio by causing changes in the flow circulation about the wing can not be found directly from the wing lift and drag coefficients as presented in figures 3 and 4, respectively. In order to determine the effectiveness of the jet, effective lift-drag ratios, $(L/D)_e$, for the various configurations were obtained by subtracting the jet-reaction coefficients from the measured wing lift and drag coefficients given in figures 3 and 4. Typical curves of $(L/D)_e$ as a function of C_L for constant momentum coefficient are shown in figure 8 for configurations 1 and 2. These data and those for configurations 3 to 5 showed increases in maximum effective lift-drag ratio with increase in momentum coefficient. For values of measured lift coefficient below C_L for $(L/D)_{e,max}$, use of the jet generally decreased the effective lift-drag ratio.

The increment in $(L/D)_{e,max}$ due to the jet for each configuration is shown in figure 9 as a function of momentum coefficient. The largest increase in $(L/D)_{e,max}$ occurred for configuration 1 at a value of C_μ of approximately 0.020 and was about 10 percent of the jet-inoperative value of $(L/D)_{max}$. These data (fig. 9) indicate that the most effective jet inclinations are those nearer the vertical with decreasing effectiveness as the jet is inclined rearward $(\delta_j \rightarrow 180^\circ)$.

Reducing the span of the jet decreased the effectiveness of the jet in increasing $(L/D)_{e,max}$ (configurations 4 and 5 in fig. 9). Configurations 4 and 5 had the same span but the jet of configuration 5 was located farther inboard. Of the two, configuration 5 was more effective.

In order to examine the factors affecting the observed increases in maximum effective lift-drag ratio, the incremental changes in $C_{L,e}$ and $C_{D,e}$ due to the jet at $\alpha = 4^\circ$ $\left(\text{near } (L/D)_{max}\right)$ are plotted in figure 10 for configurations 1, 2, and 3. For momentum coefficients less than 0.020, the increases in $(L/D)_{e,max}$ are due to increases in $C_{L,e}$. However, the limited data for values of C_μ greater than 0.020 indicate that increases in $C_{D,e}$ contribute to the reduction in $\Delta(L/D)_{e,max}$ observed at these higher momentum coefficients. (See fig. 9.)

Practical Applications

The foregoing analysis indicates that some improvement in $(L/D)_{e,max}$ can be obtained by the use of a jet. Since the largest improvement indicated by the present investigation is about 10 percent of the maximum lift-drag ratio for the jet-inoperative condition, the practical aspects of the use of a jet with a complete airplane should be considered.

One source of supply for the jet is a jet-engine exhaust. In a practical engine installation an inlet area of 1 percent of the wing area would be reasonable for $M = 2$. The mass flow at full thrust for this assumption would correspond to a momentum coefficient of 0.020 in the present investigation. The variation of wing drag coefficient with lift coefficient for the jet-inoperative condition and for jet deflections of 110° and 150° at $C_\mu \approx 0.020$ and $R = 2.8 \times 10^6$ are shown in figure 11. A jet with a deflection angle of 150° produced the largest thrust of all the configurations tested. However, at this deflection angle there was still insufficient thrust to overcome the drag of the wing alone at the value of C_L for $(L/D)_{e,max}$ $\left(C_L \approx 0.17\right)$. (See fig. 11.) The addition of the body, engine nacelle, and tail drag and the requirements for maneuvering thrust would make this deficiency larger. Furthermore, as previously discussed, the more rearwardly inclined jets are the least effective in increasing $(L/D)_{e,max}$. For an actual engine installation the ratio of exit area to inlet area should be of the order of $1\frac{1}{2}$ and not approximately 1/3 as found in the present investigation. Thus, the use of the engine exhaust to supply the jet does not appear feasible.

Another source of supply for the jet would be engine bypass air. In this approach not only would the mass flow of air available for the jet be small but also the momentum of the air would decrease because of inlet and ducting losses. Therefore, it appears that gains from this approach would not be large enough to warrant the increased complexity of the airplane.

CONCLUSIONS

An investigation has been made at a Mach number of 2.01 to determine the effects of a jet on the lower surface of a 45° sweptback wing on the lift-drag ratio. The conclusions are indicated as follows:

1. The jet produces gains in lift-drag ratio at and near the maximum lift-drag ratio but actually decreases the lift-drag ratio at the lower operating lift coefficients.

2. The most effective jet inclinations appear to be those nearer the vertical with decreasing effectiveness as the jet is inclined rearward.

3. The improvement in maximum lift-drag ratio does not appear to be large enough to be of practical use on an actual airplane because of the problems arising from trying to provide a source of air for the jet.

Langley Research Center,
National Aeronautics and Space Administration,
Langley Field, Va., August 31, 1959.

REFERENCE

1. Lord, Douglas R.: Aerodynamic Characteristics of Several Jet-Spoiler Controls on a 45° Sweptback Wing at Mach Numbers of 1.61 and 2.01. NACA RM L58D18, 1958.

TABLE I

CONFIGURATIONS TESTED

Configuration	δ_j, deg	$\frac{2b_j}{b}$	$\frac{2y_i}{b}$	$\frac{2y_o}{b}$	Slot width, in.	Slot length, in.
1	110	0.58	0.19	0.77	0.050	1.00
2	130	.58	.19	.77	.050	1.00
3	150	.57	.20	.77	.054	1.00
4	130	.40	.37	.77	.050	1.00
5	130	.40	.19	.59	.050	1.00

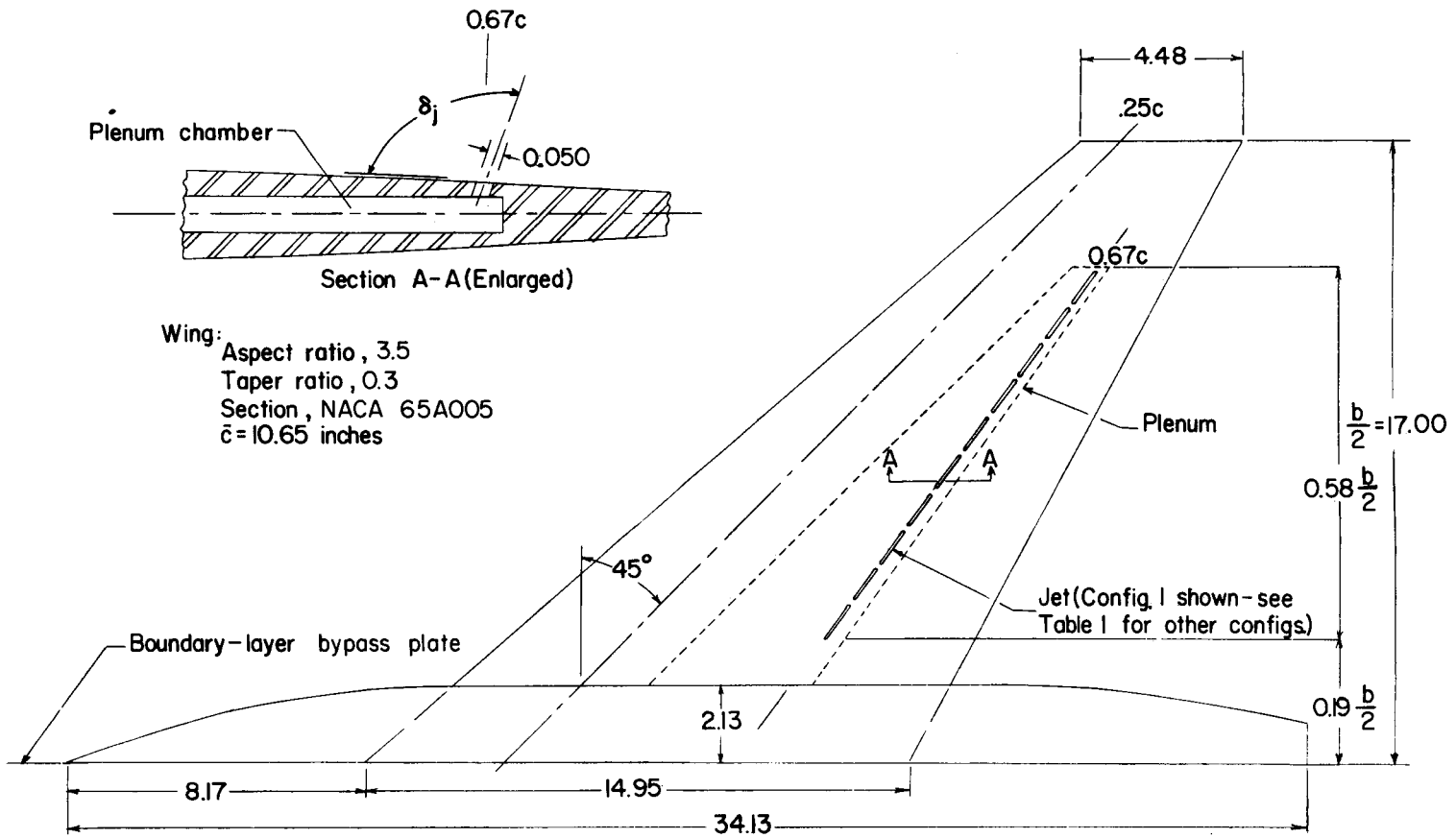

Figure 1.- Sketch showing lower surface of semispan-wing—fuselage model. All dimensions are in inches.

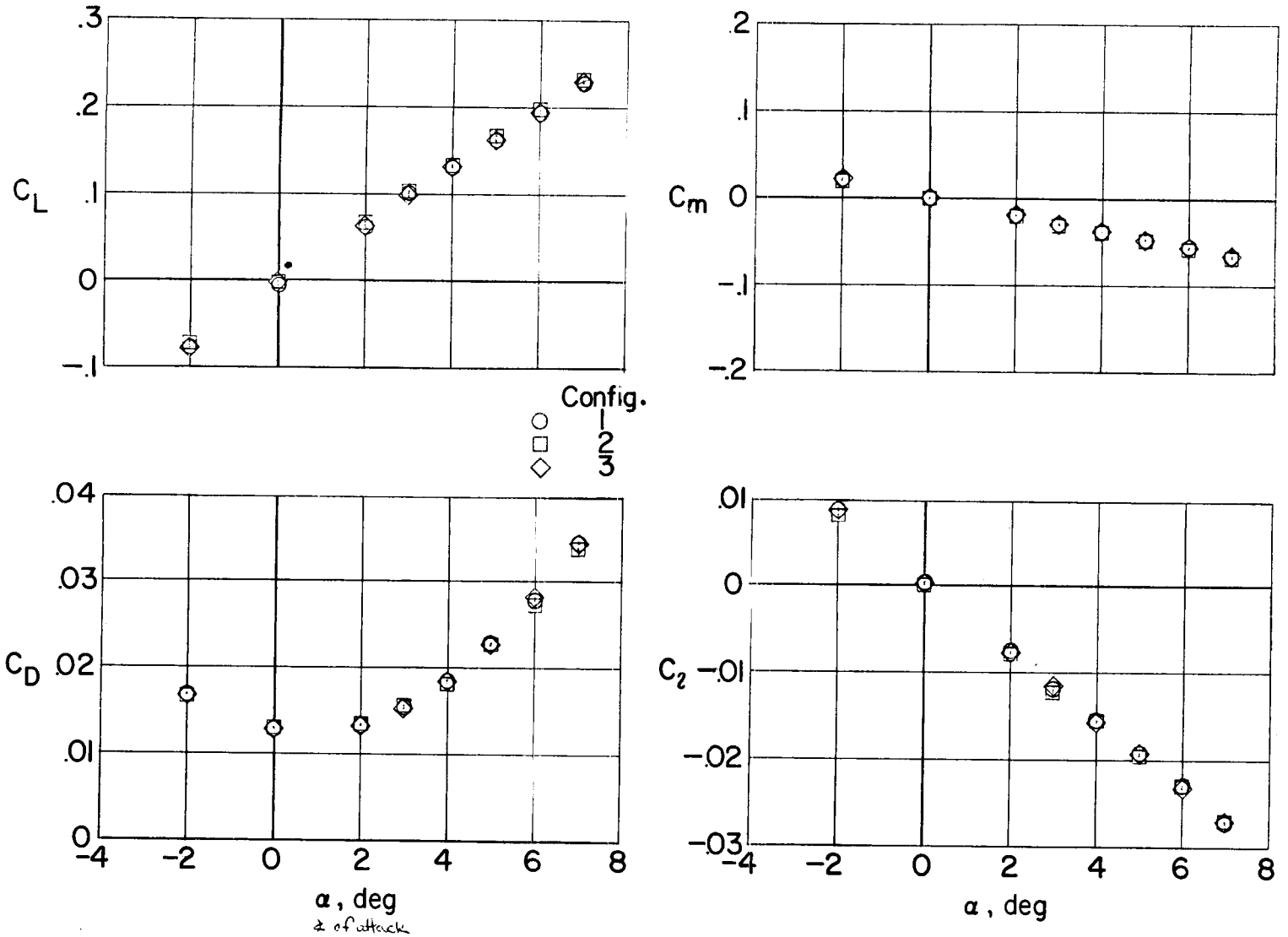

Figure 2.- Aerodynamic characteristics of wing with jet inoperative. $R = 2.8 \times 10^6$.

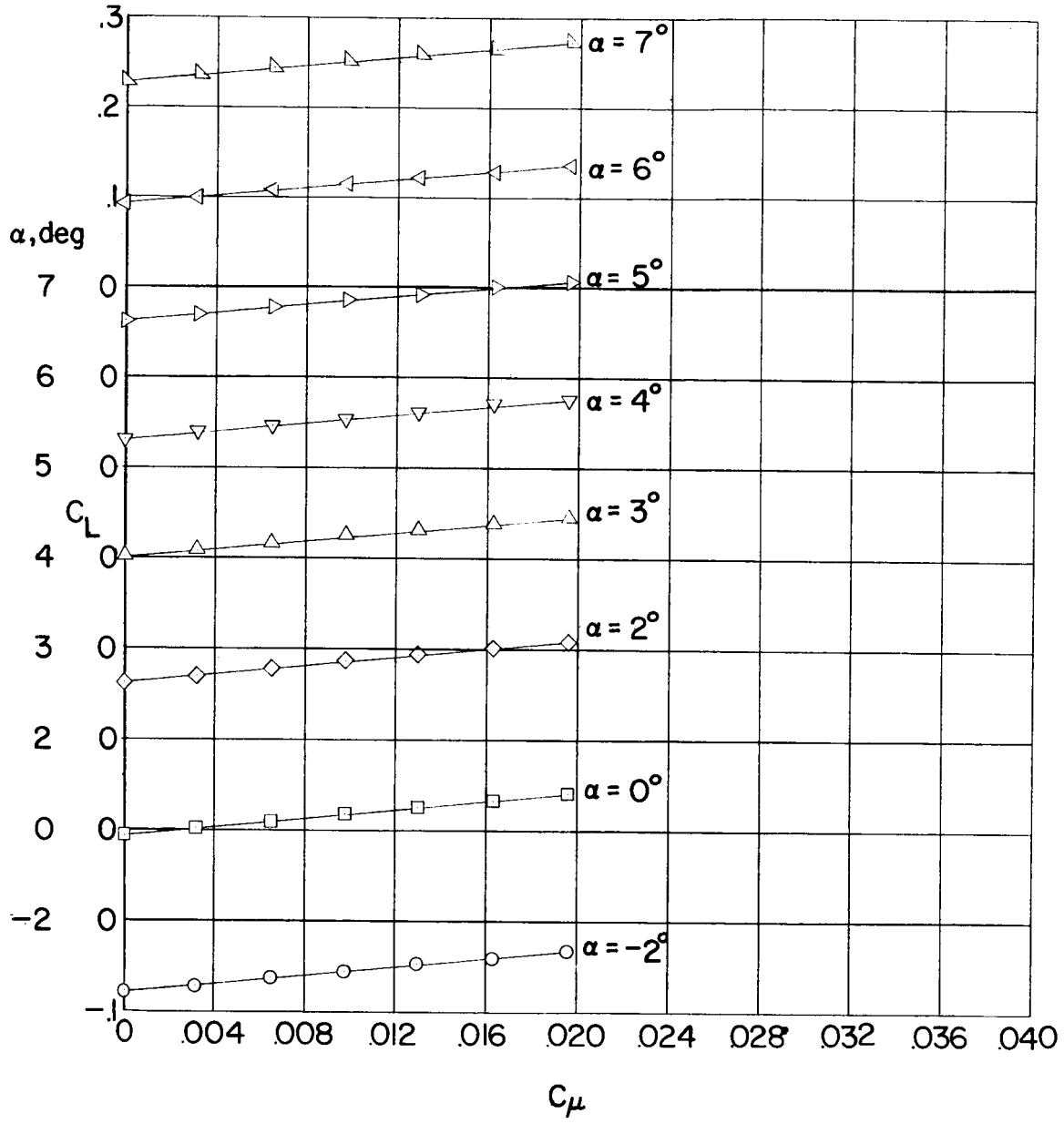

(a) Configuration 1; $R = 2.8 \times 10^6$.

Figure 3.- Variation of wing lift coefficient with momentum coefficient.

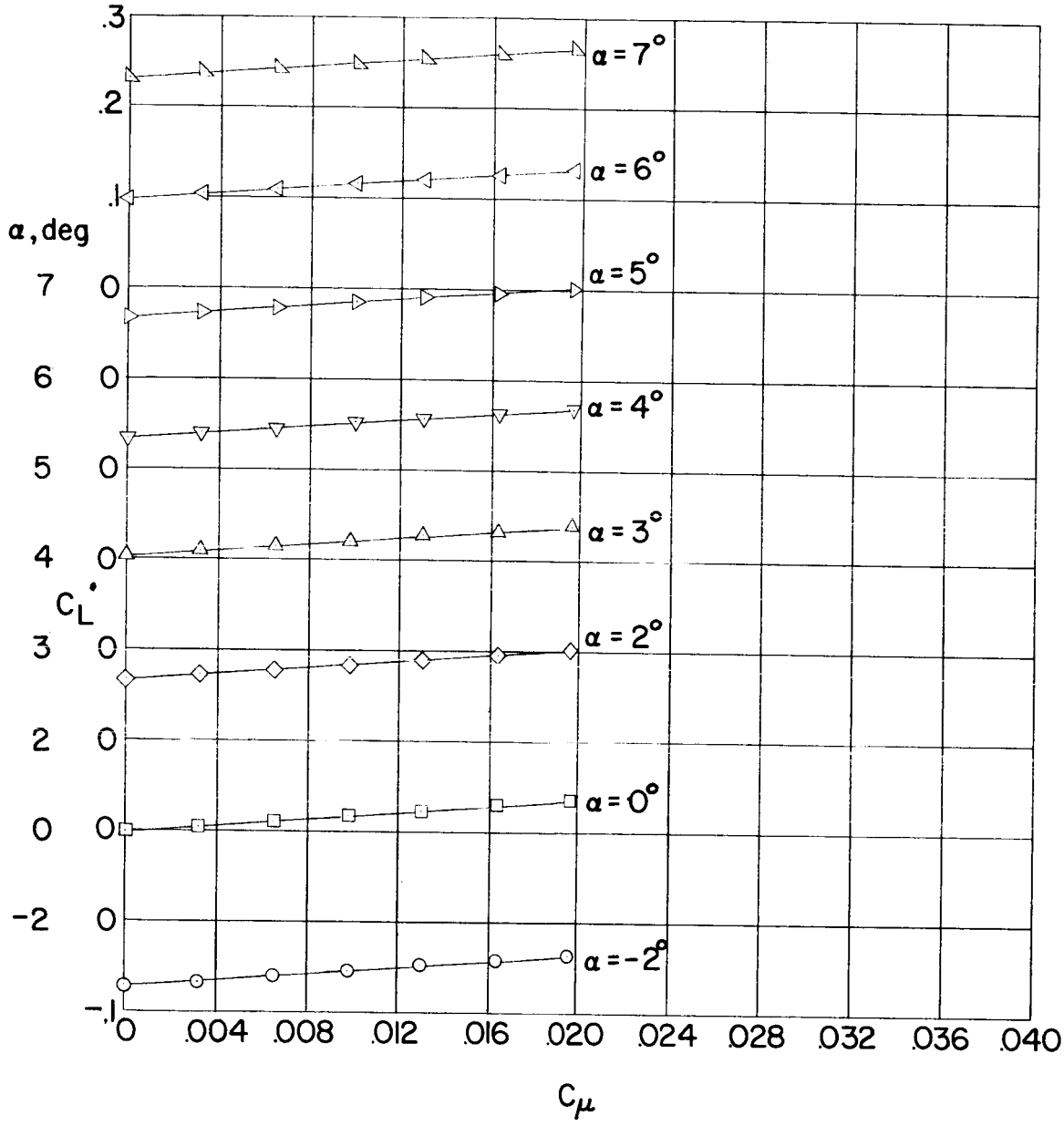

(b) Configuration 2; $R = 2.8 \times 10^6$.

Figure 3.- Continued.

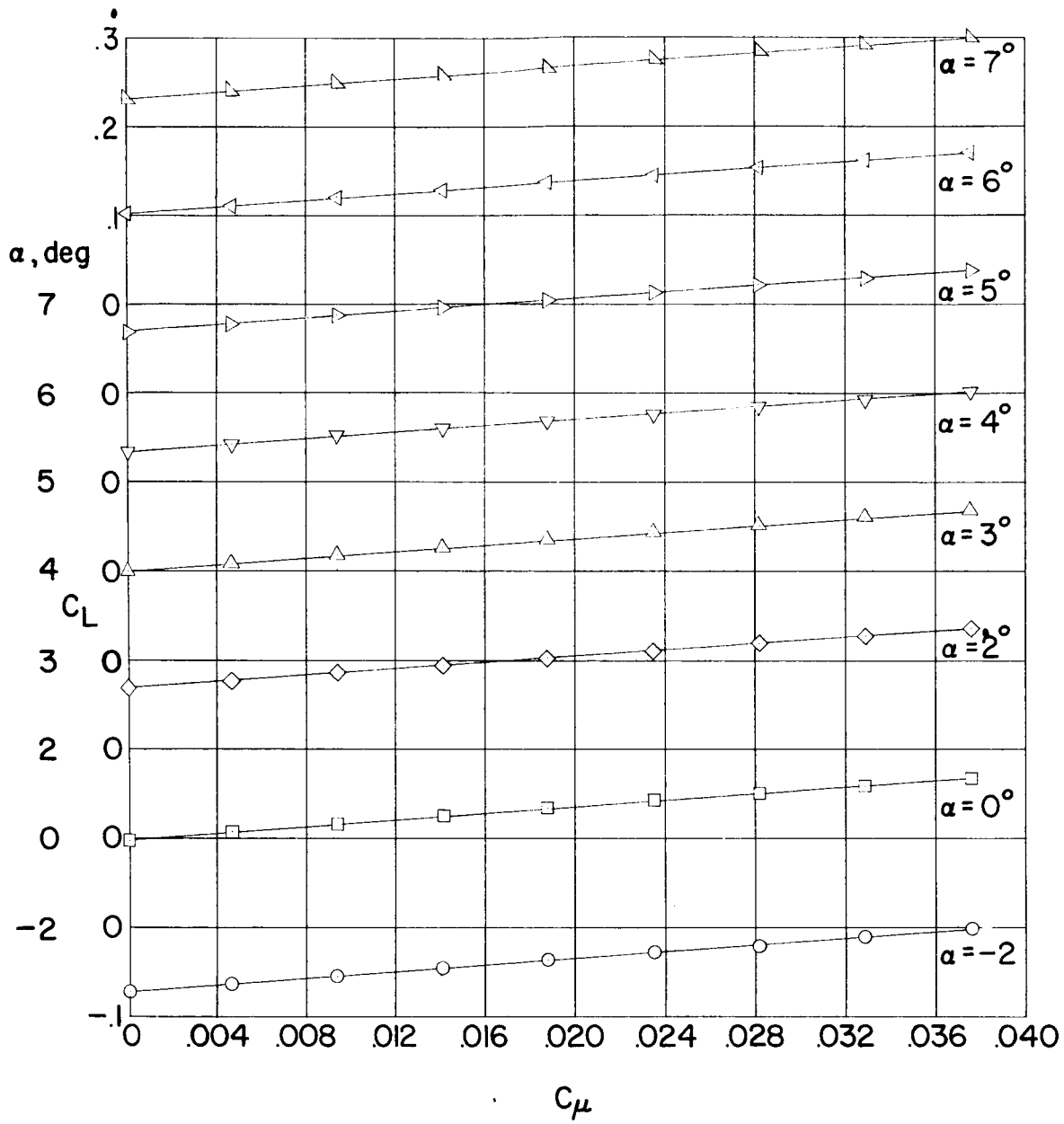

(c) Configuration 2; R = 1.5×10^6.

Figure 3.- Continued.

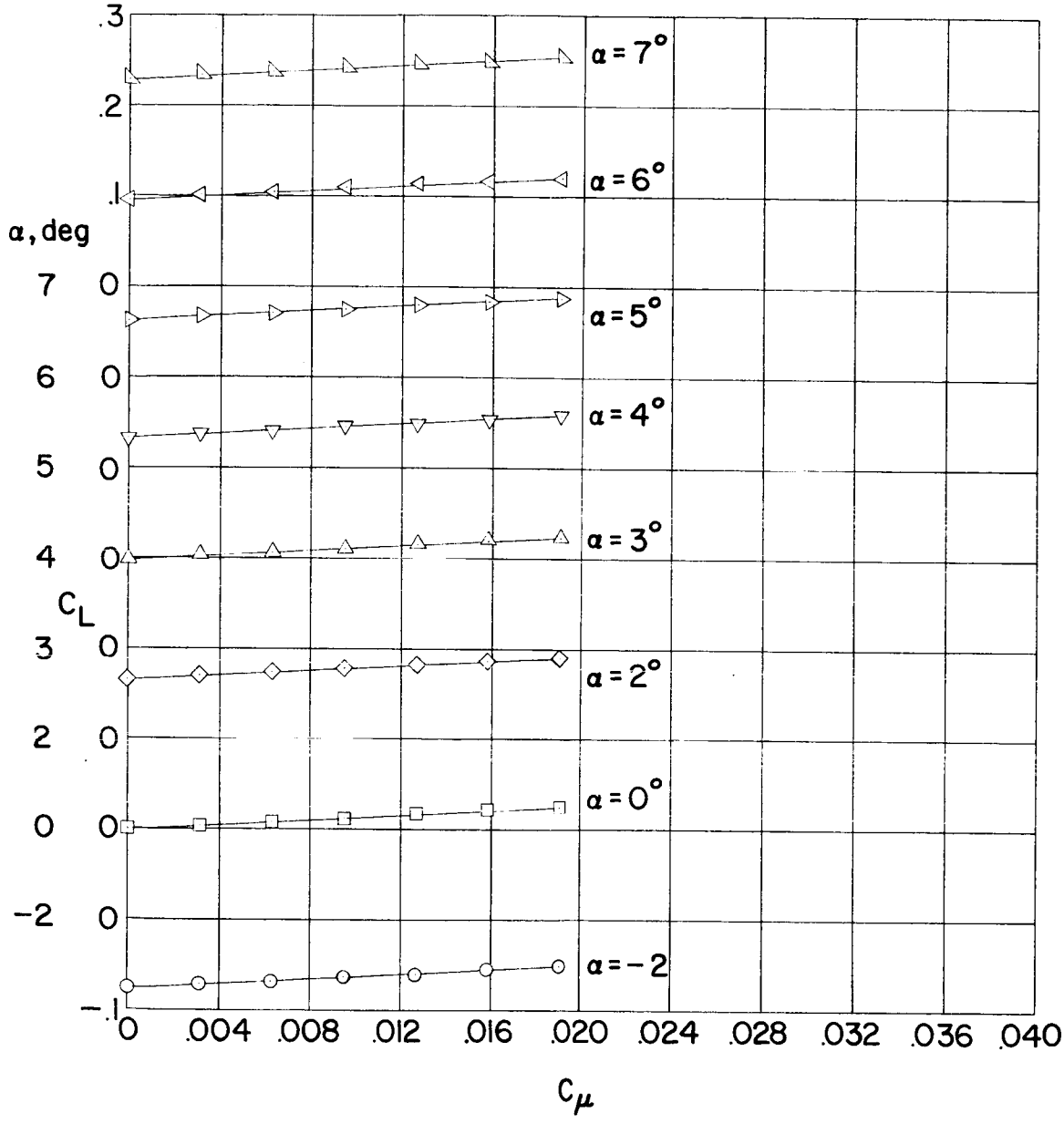

(d) Configuration 3; R = 2.8×10^6.

Figure 3.- Continued.

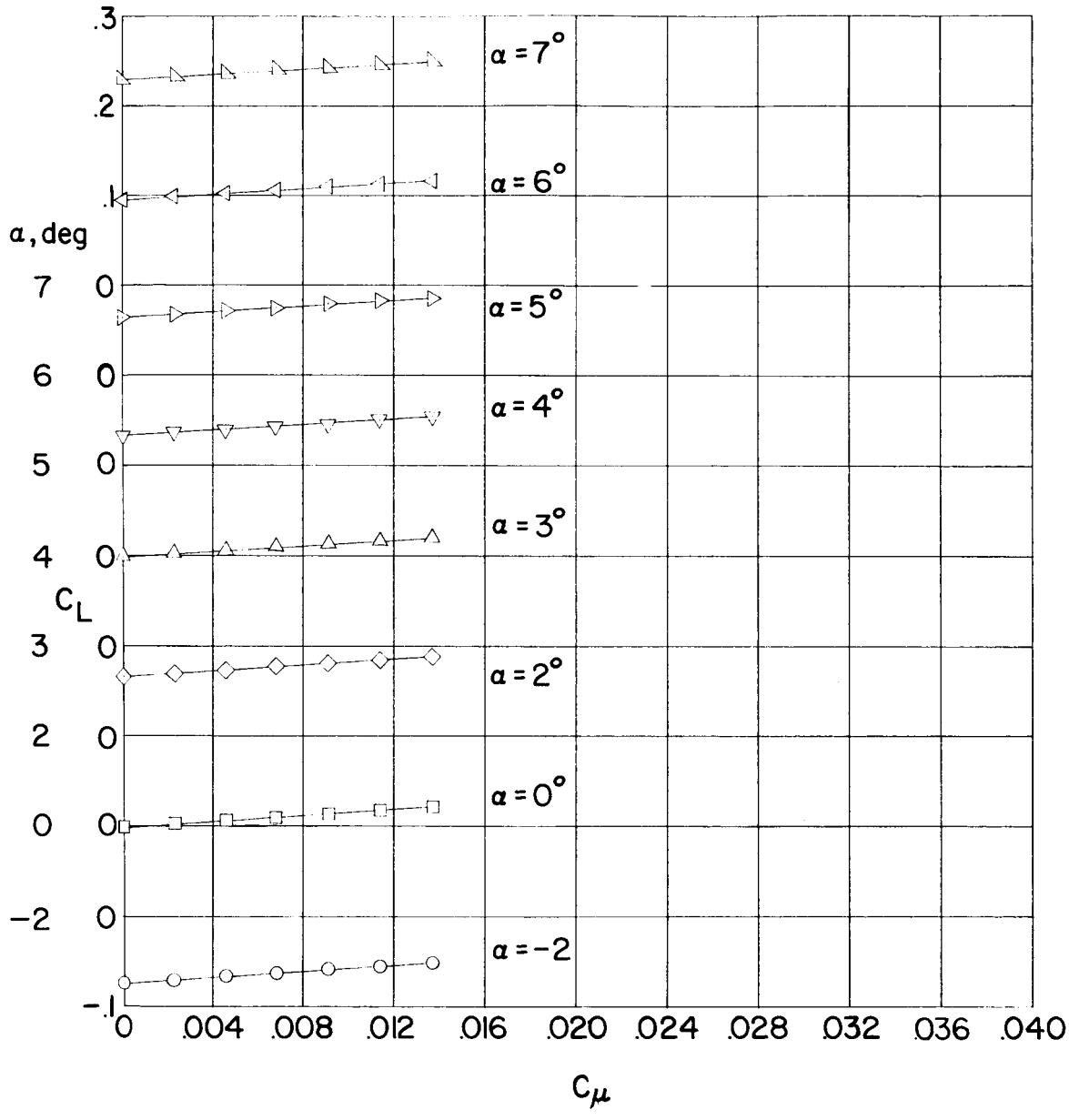

(e) Configuration 4; $R = 2.8 \times 10^6$.

Figure 3.- Continued.

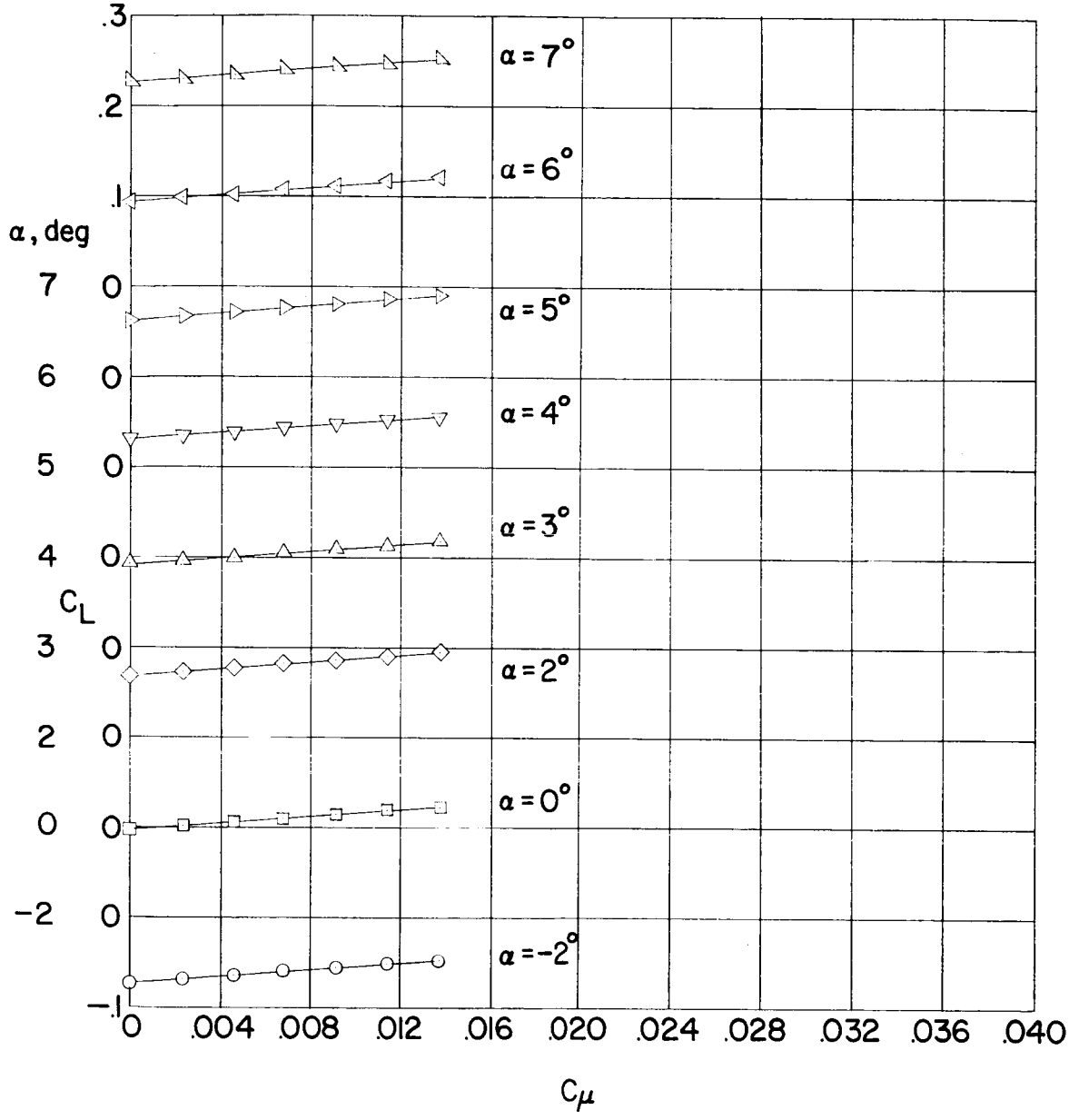

(f) Configuration 5; $R = 2.8 \times 10^6$.

Figure 3.- Concluded.

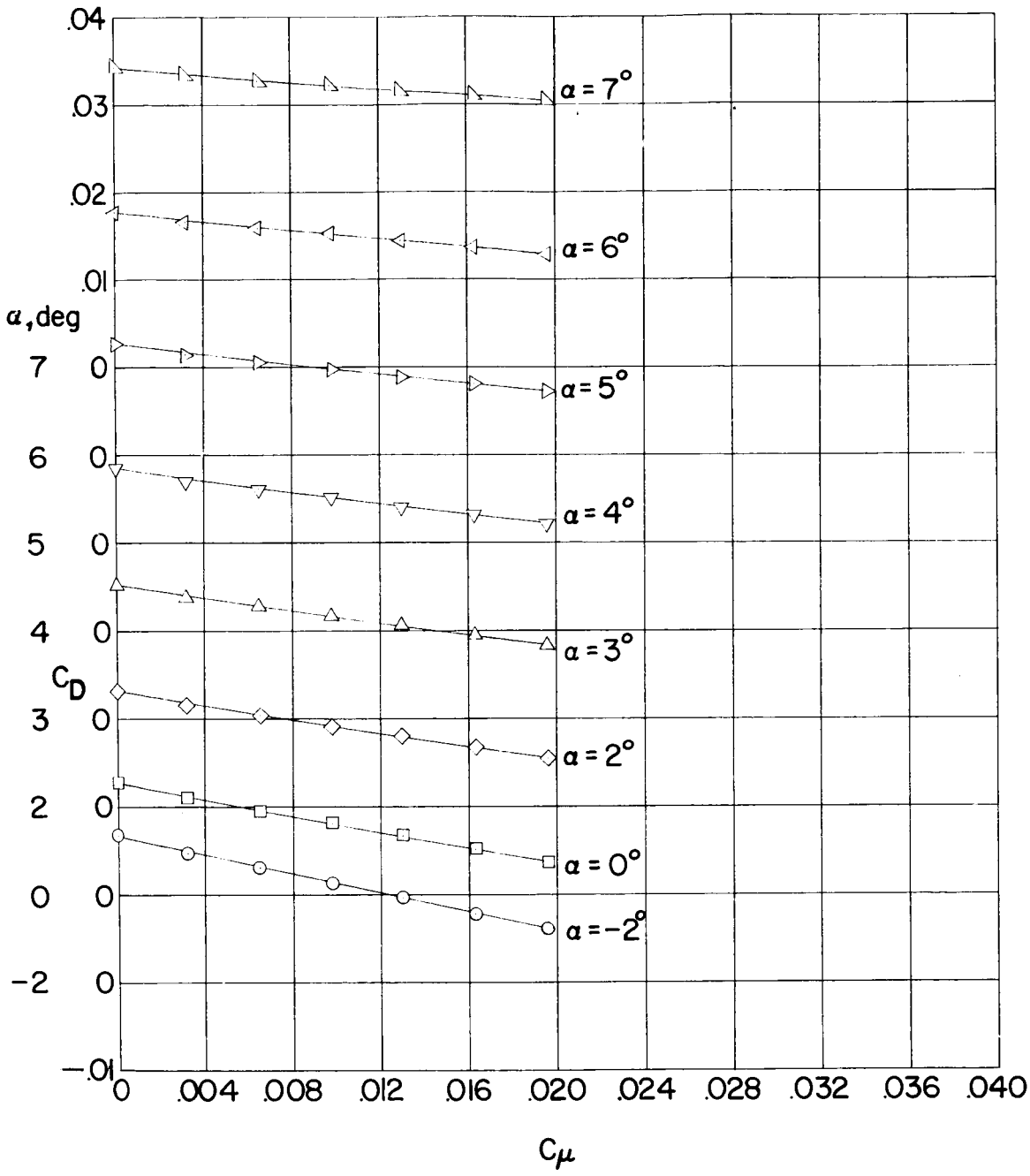

(a) Configuration 1; $R = 2.8 \times 10^6$.

Figure 4.- Variation of wing drag coefficient with momentum coefficient.

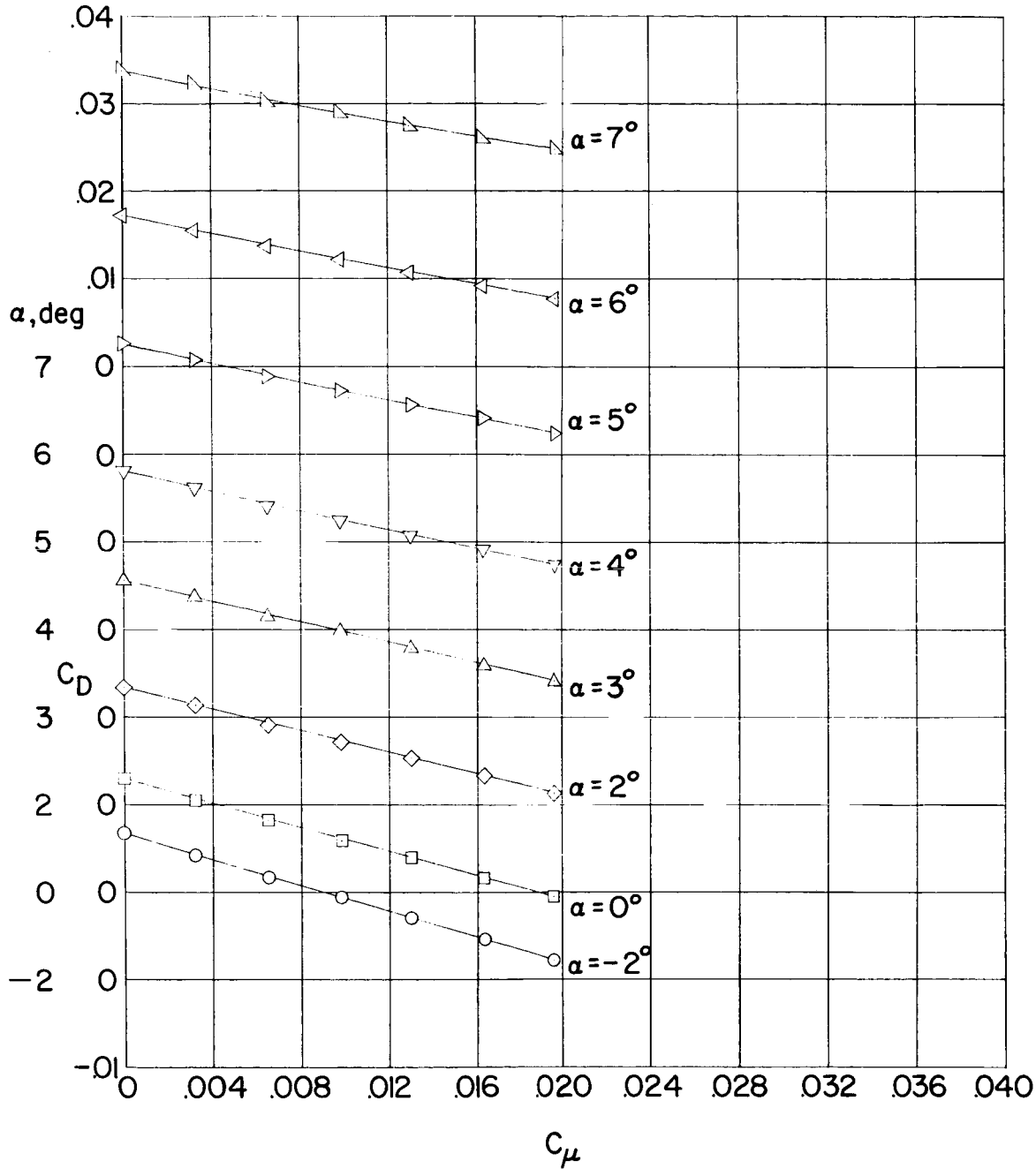

(b) Configuration 2; R = 2.8×10^6.

Figure 4.- Continued.

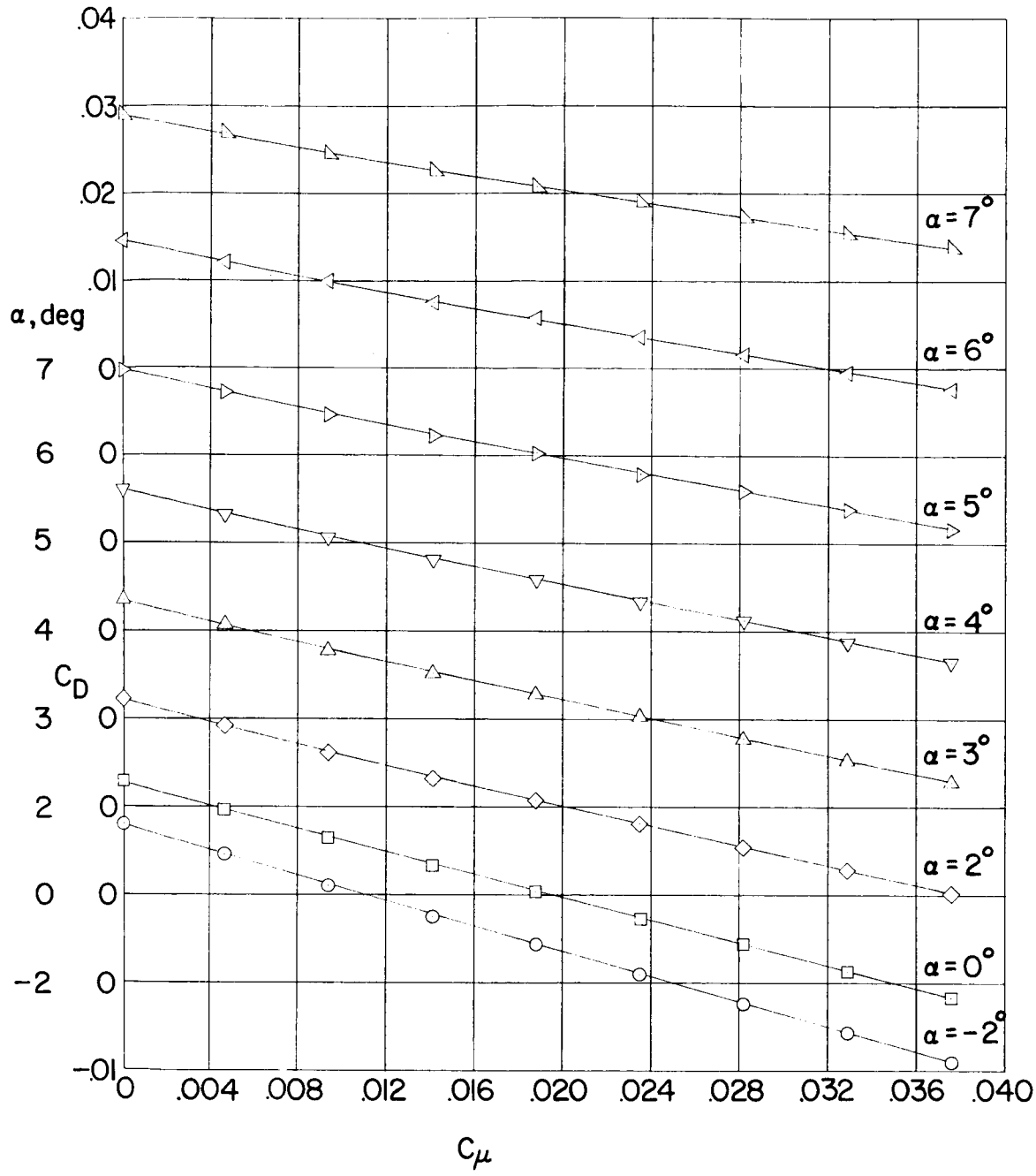

(c) Configuration 2; R = 1.5×10^6.

Figure 4.- Continued.

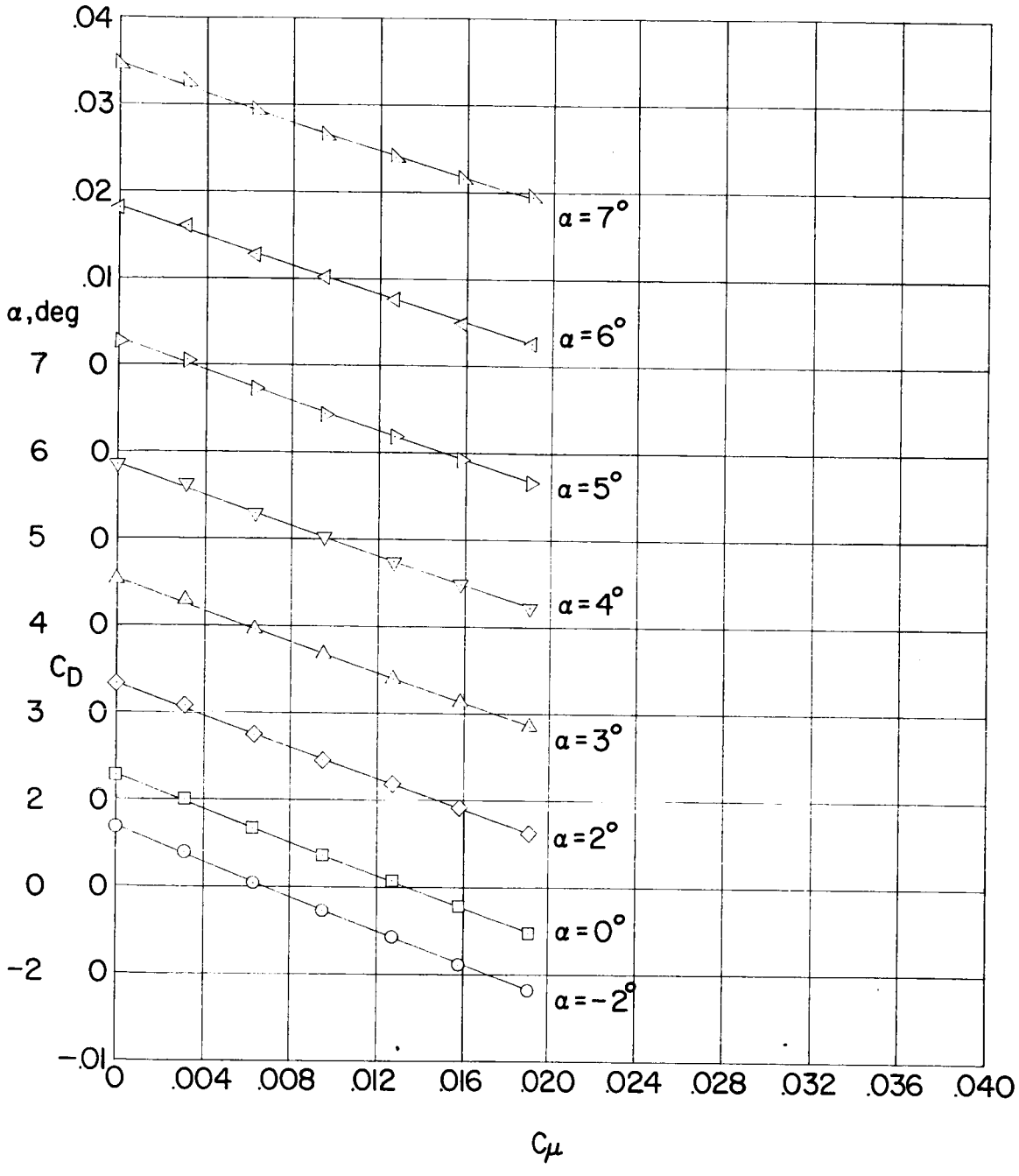

(d) Configuration 3; R = 2.8×10^6.

Figure 4.- Continued.

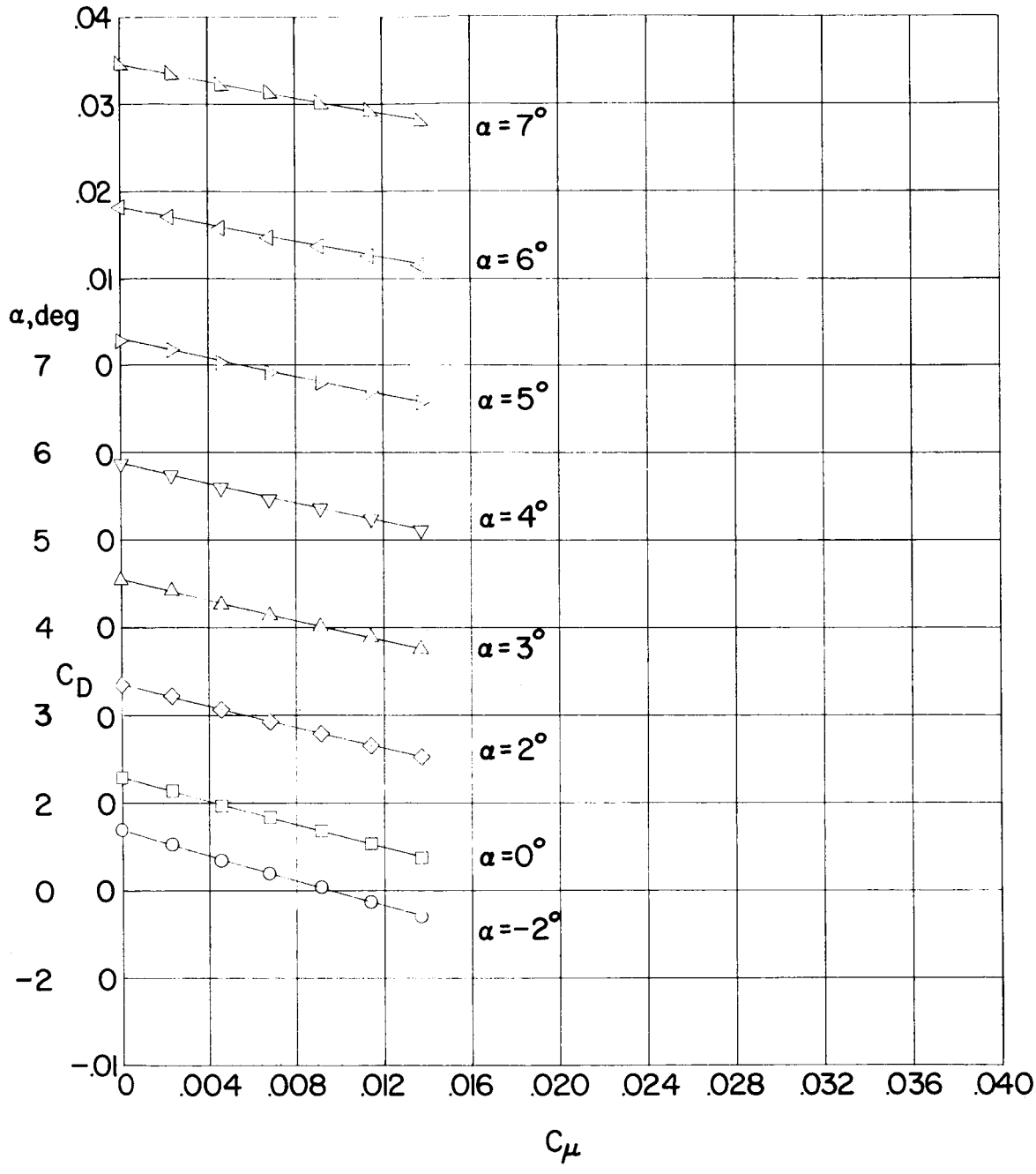

(e) Configuration 4; R = 2.8×10^6.

Figure 4.- Continued.

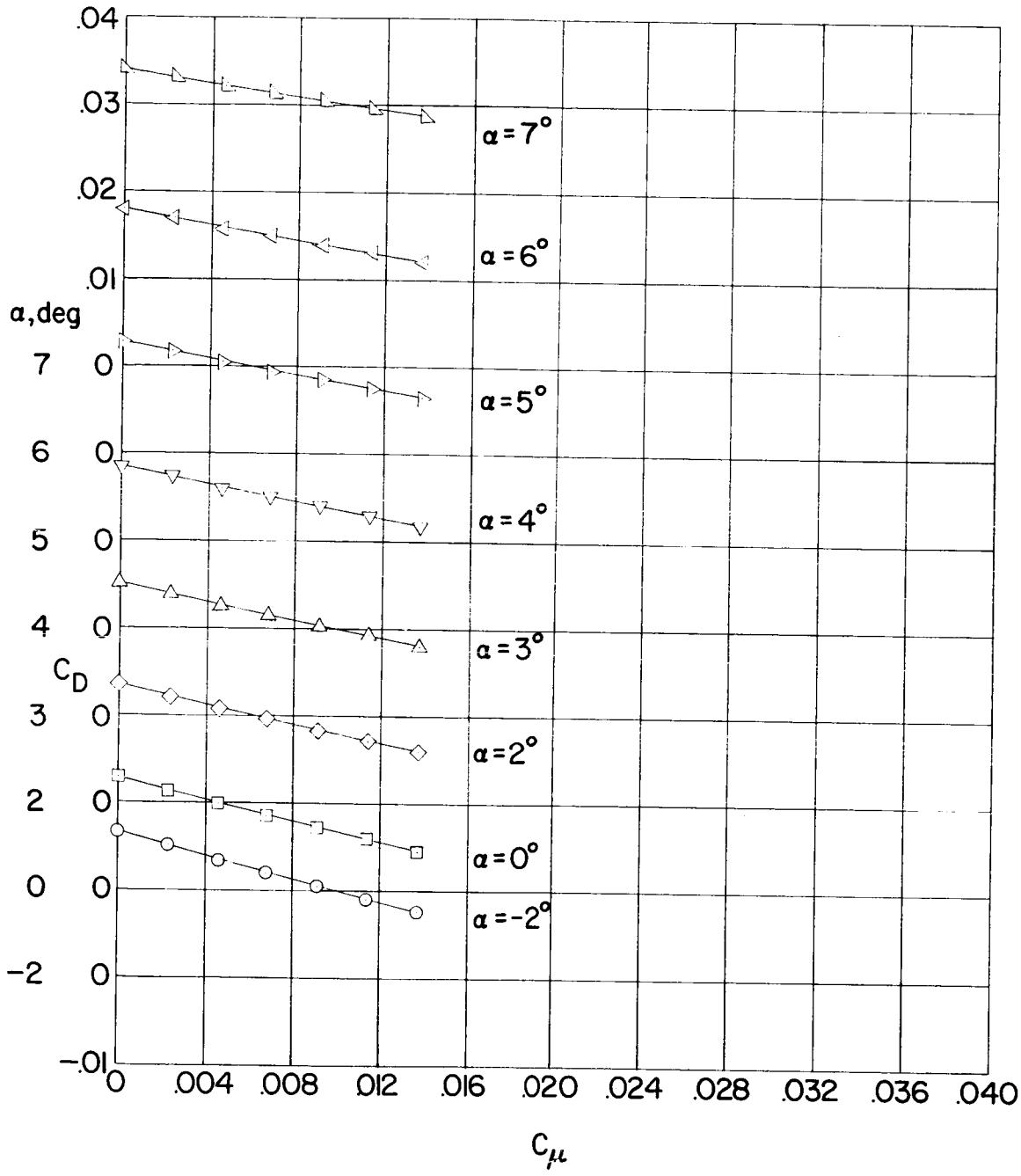

(f) Configuration 5; $R = 2.8 \times 10^6$.

Figure 4.- Concluded.

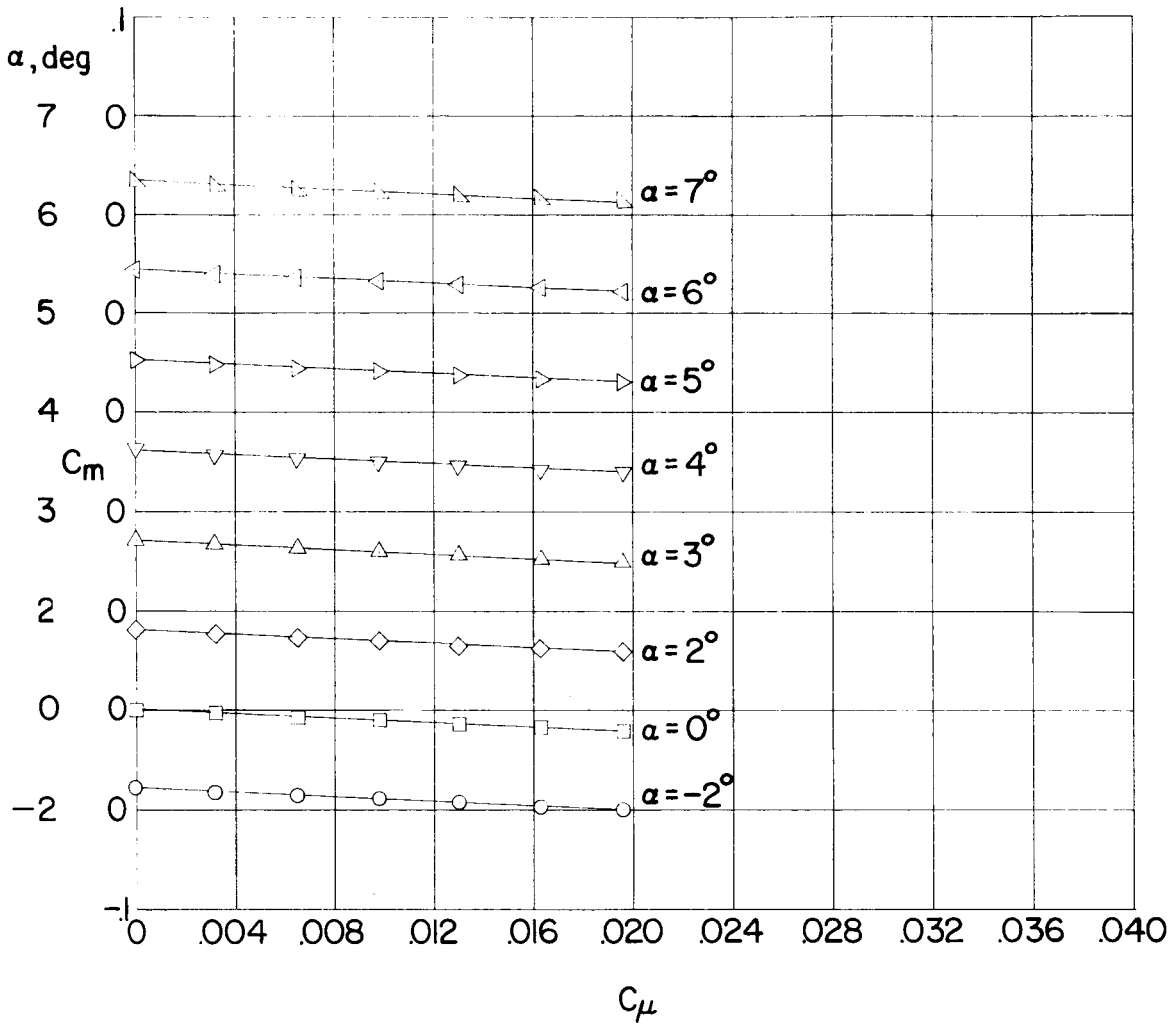

(a) Configuration 1; $R = 2.8 \times 10^6$.

Figure 5.- Variation of wing pitching-moment coefficient with momentum coefficient.

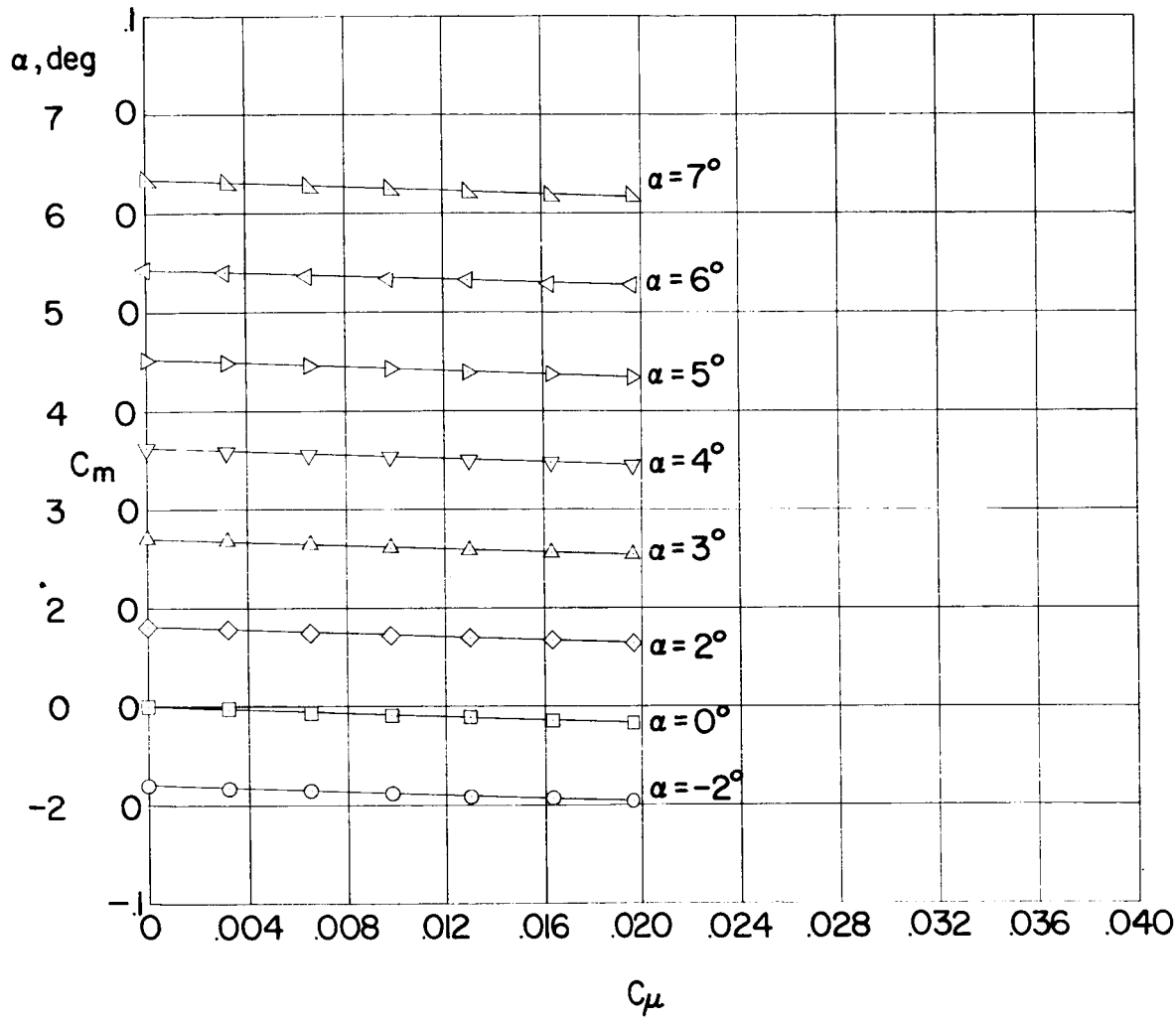

(b) Configuration 2; R = 2.8×10^6.

Figure 5.- Continued.

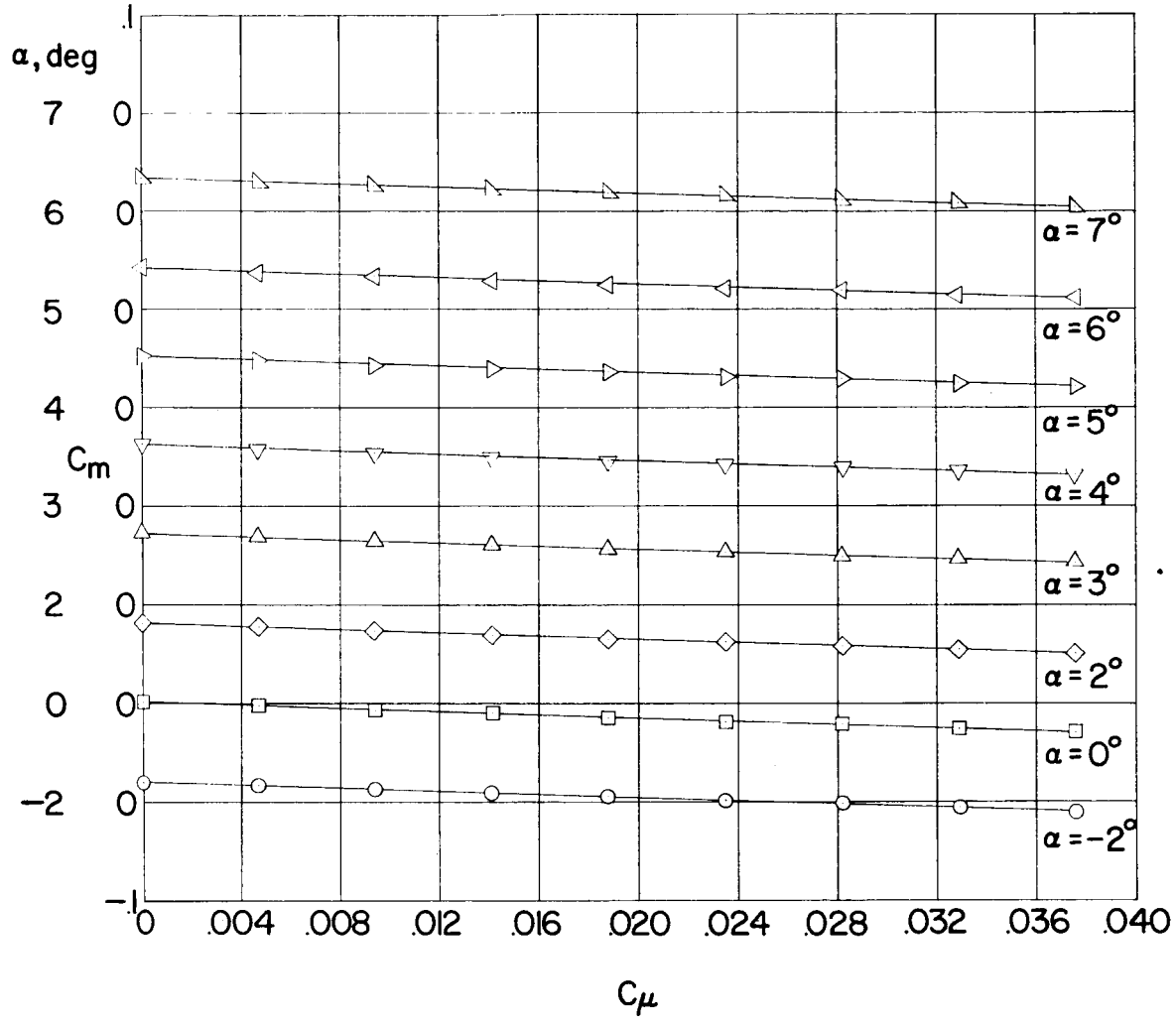

(c) Configuration 2; $R = 1.5 \times 10^6$.

Figure 5.- Continued.

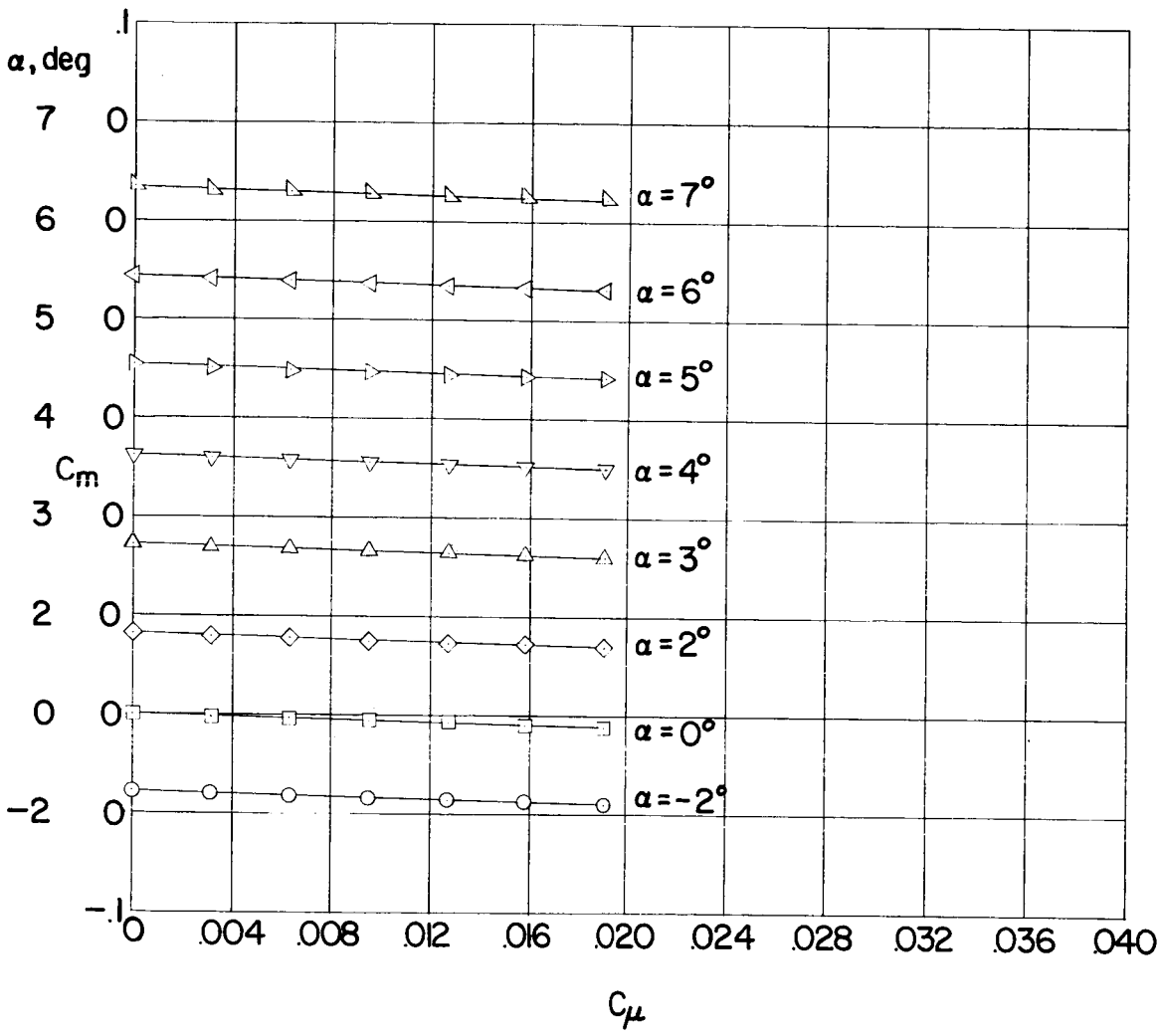

(d) Configuration 3; $R = 2.8 \times 10^6$.

Figure 5.- Continued.

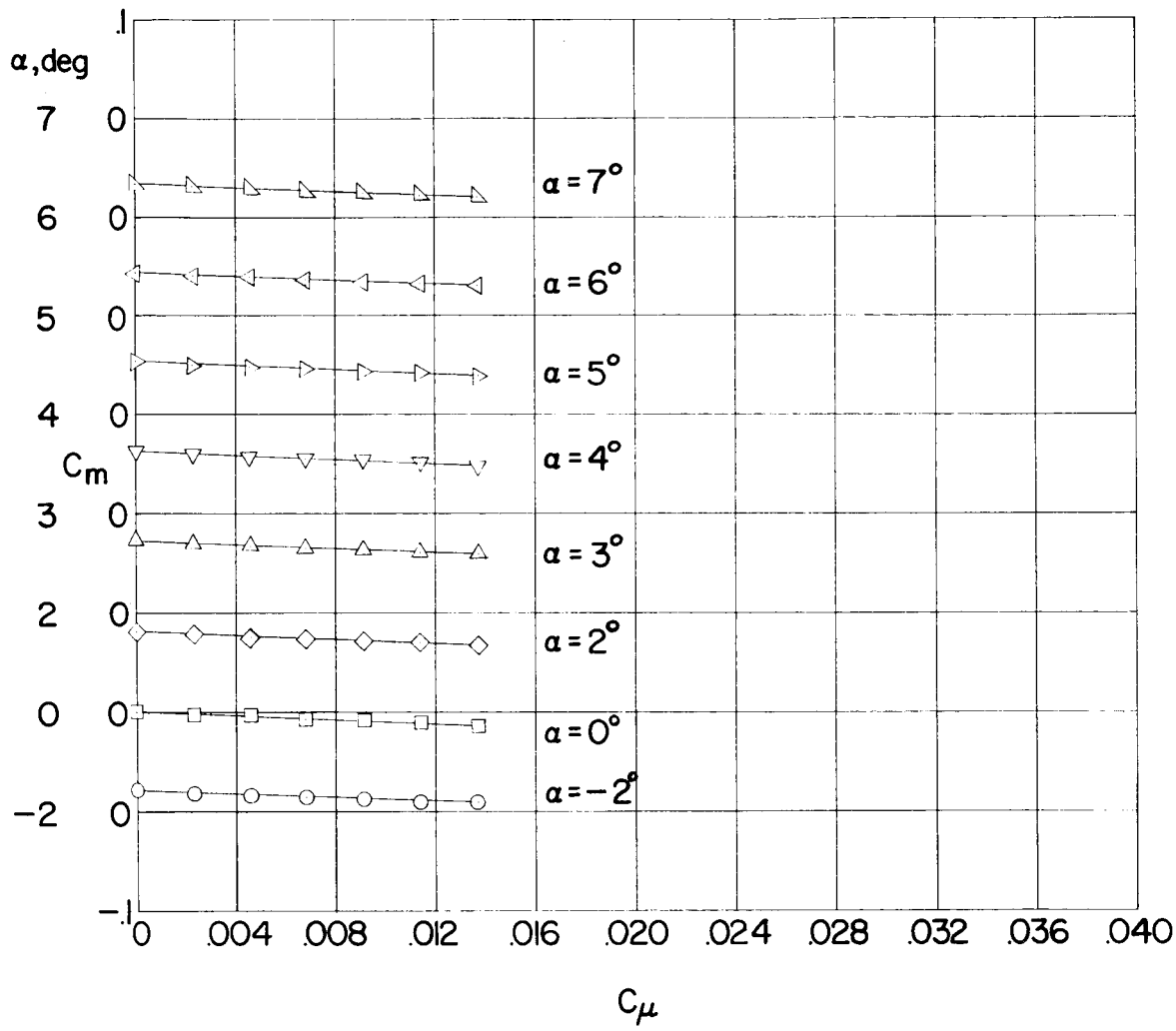

(e) Configuration 4; R = 2.8×10^6.

Figure 5.- Continued.

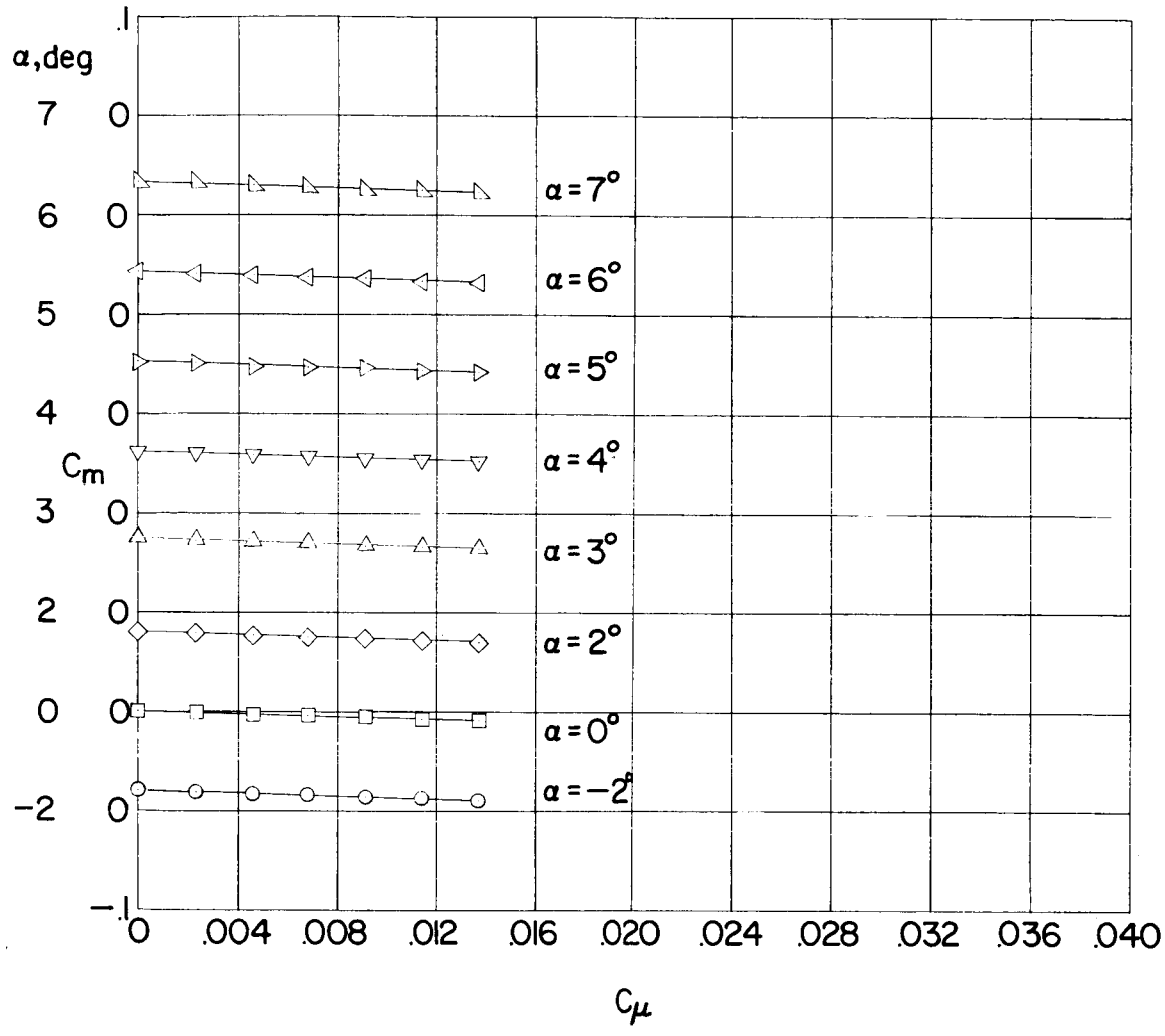

(f) Configuration 5; R = 2.8×10^6.

Figure 5.- Concluded.

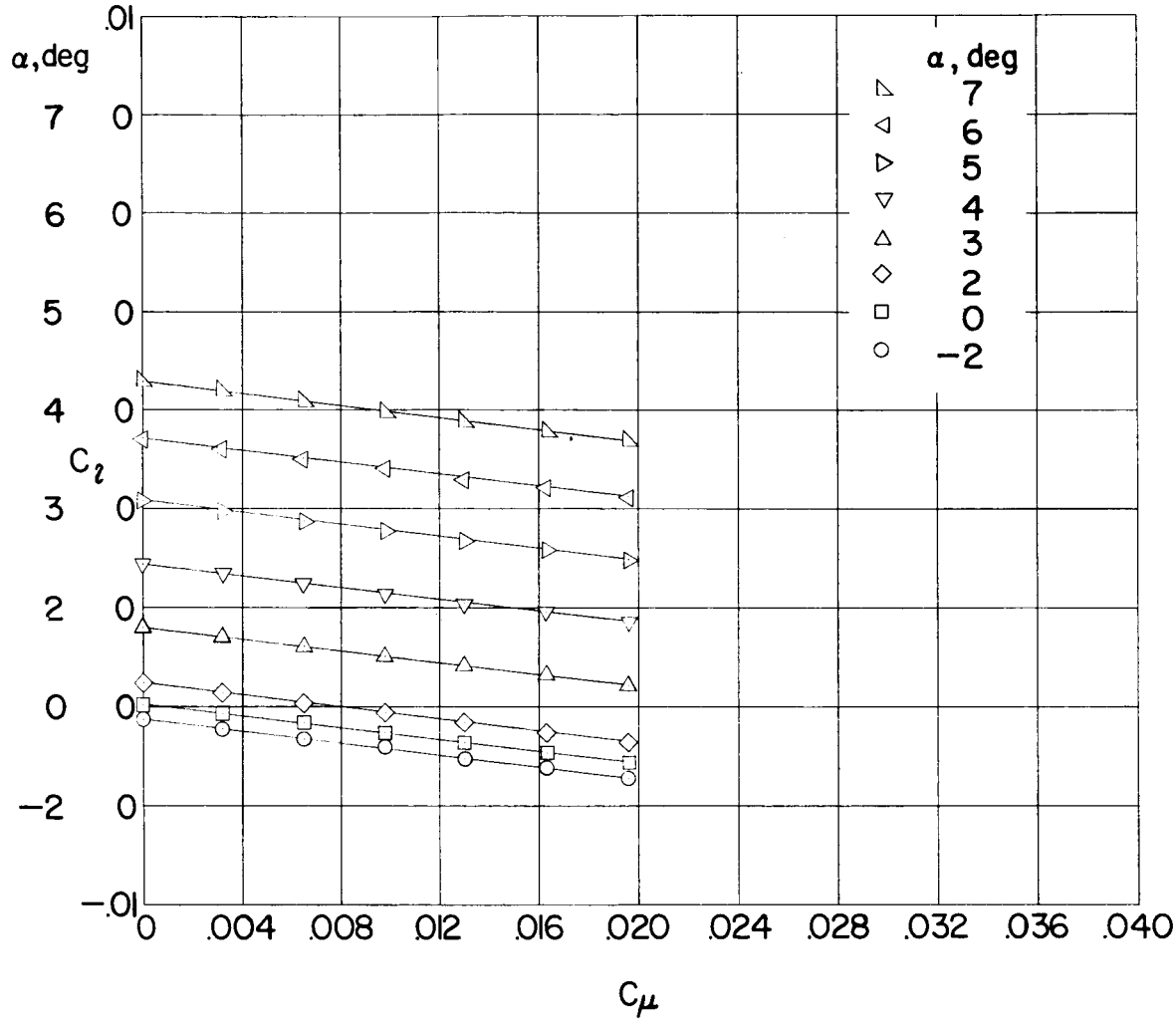

(a) Configuration 1; $R = 2.8 \times 10^6$.

Figure 6.- Variation of wing rolling-moment coefficient with momentum coefficient.

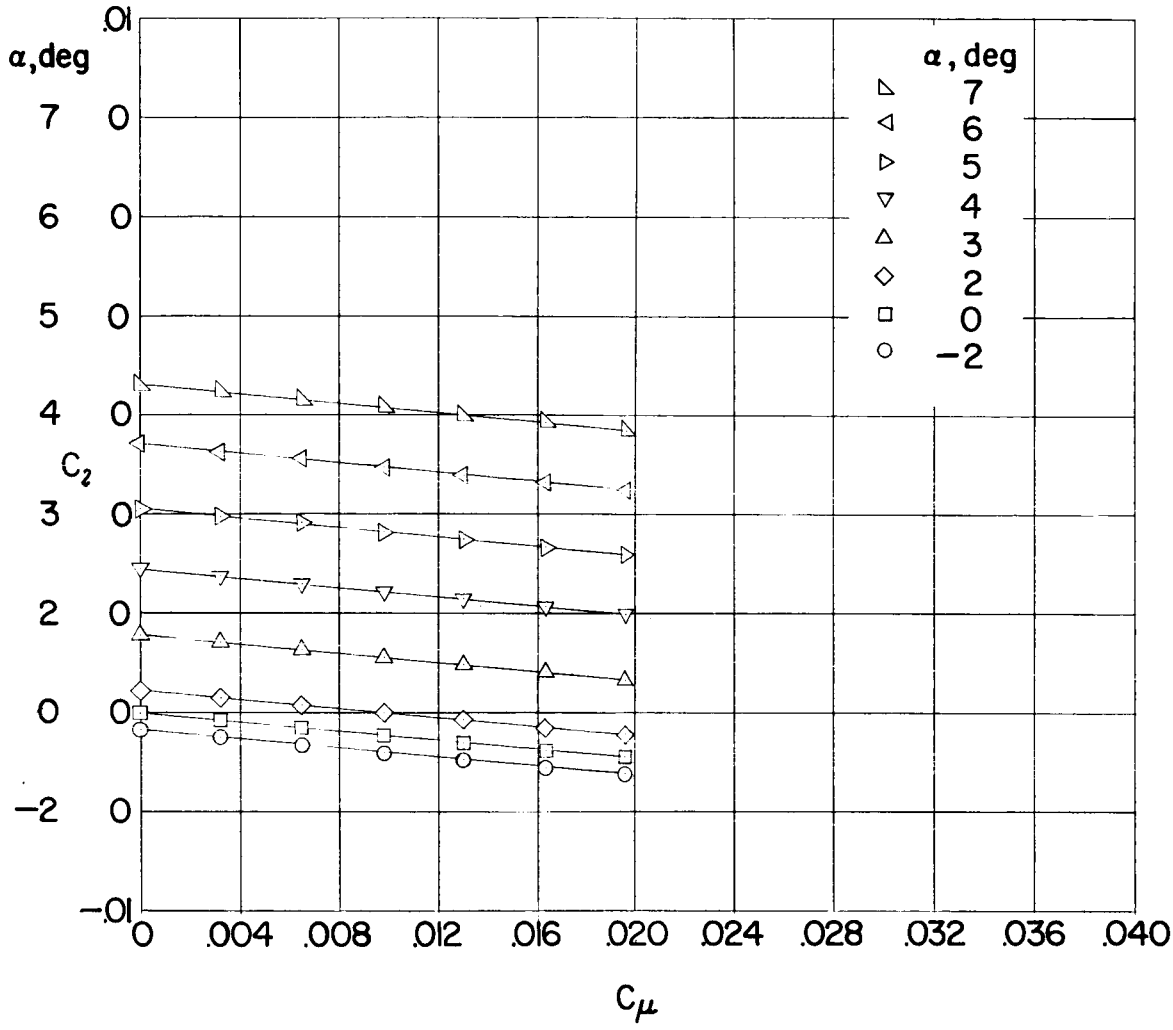

(b) Configuration 2; R = 2.8×10^6.

Figure 6.- Continued.

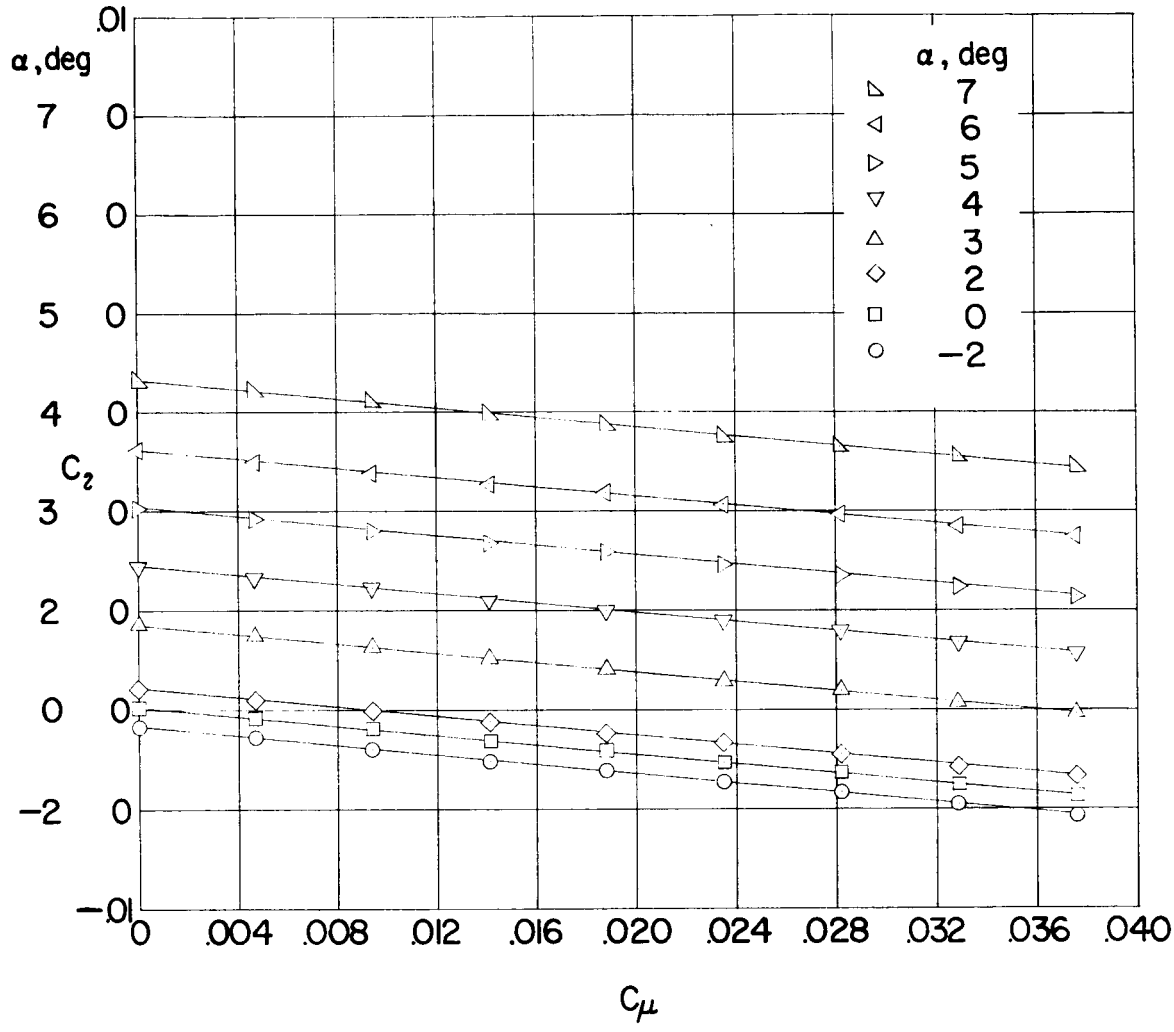

(c) Configuration 2; R = 1.5×10^6.

Figure 6.- Continued.

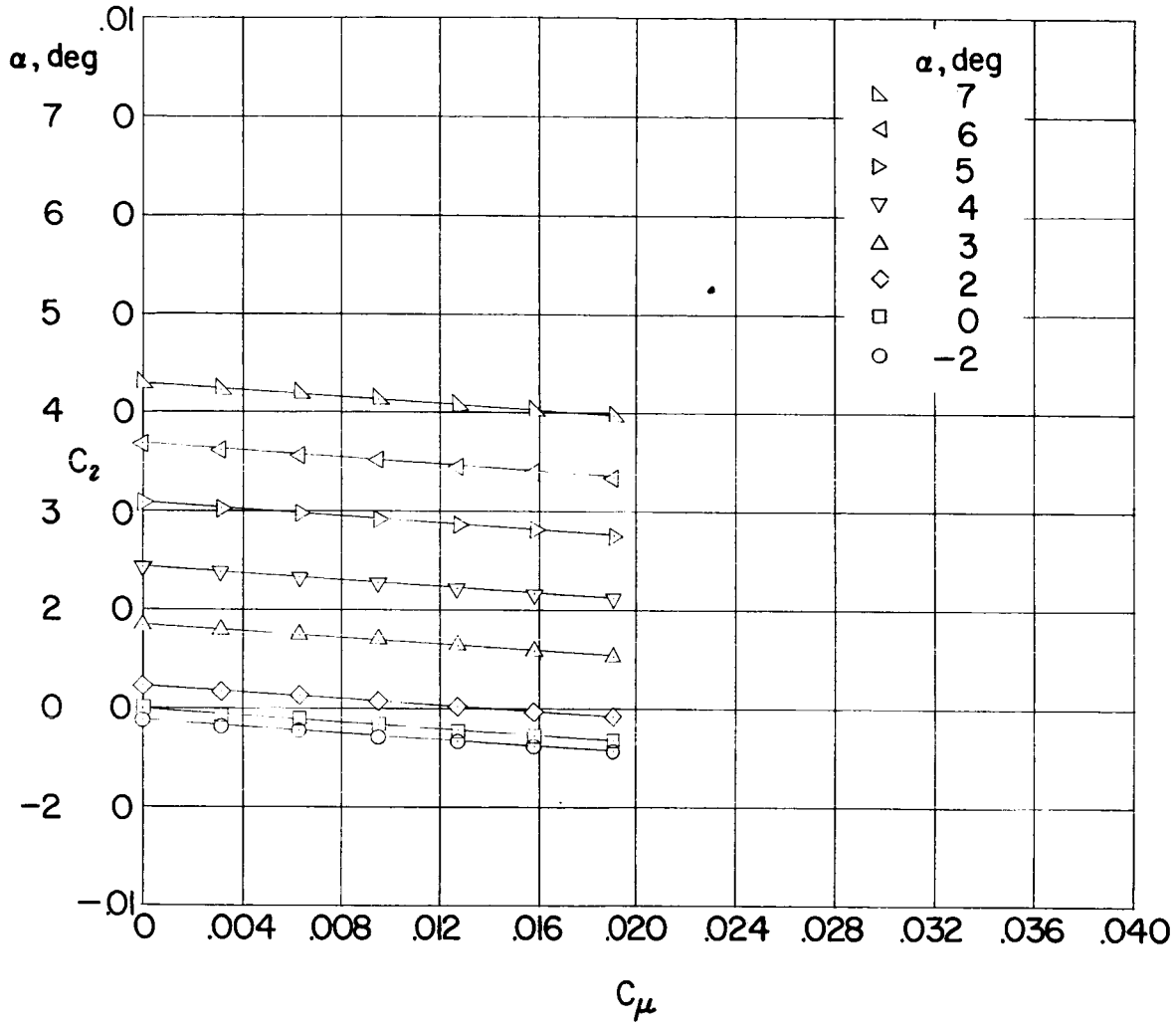

(d) Configuration 3; R = 2.8×10^6.

Figure 6.- Continued.

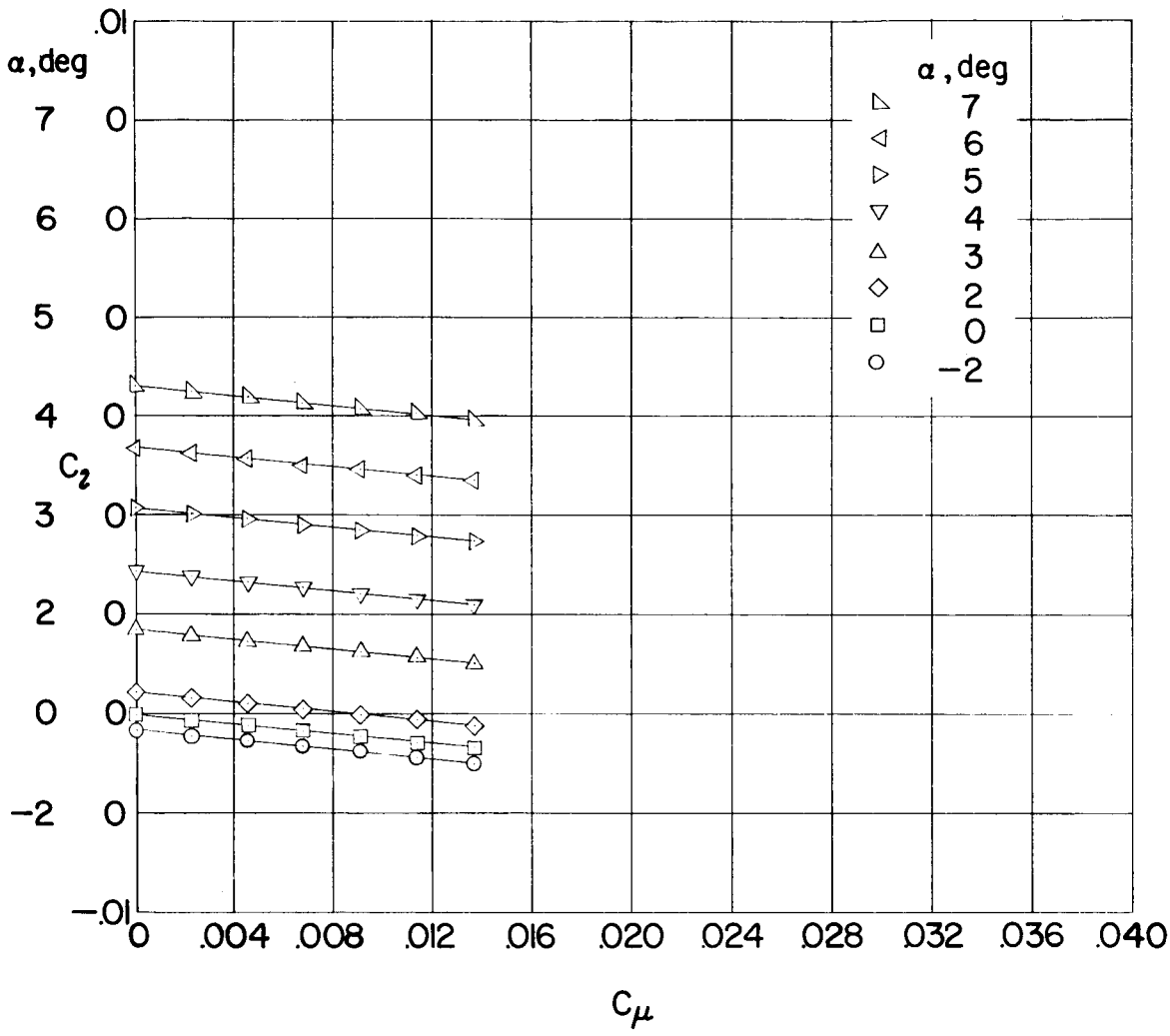

(e) Configuration 4; R = 2.8×10^6.

Figure 6.- Continued.

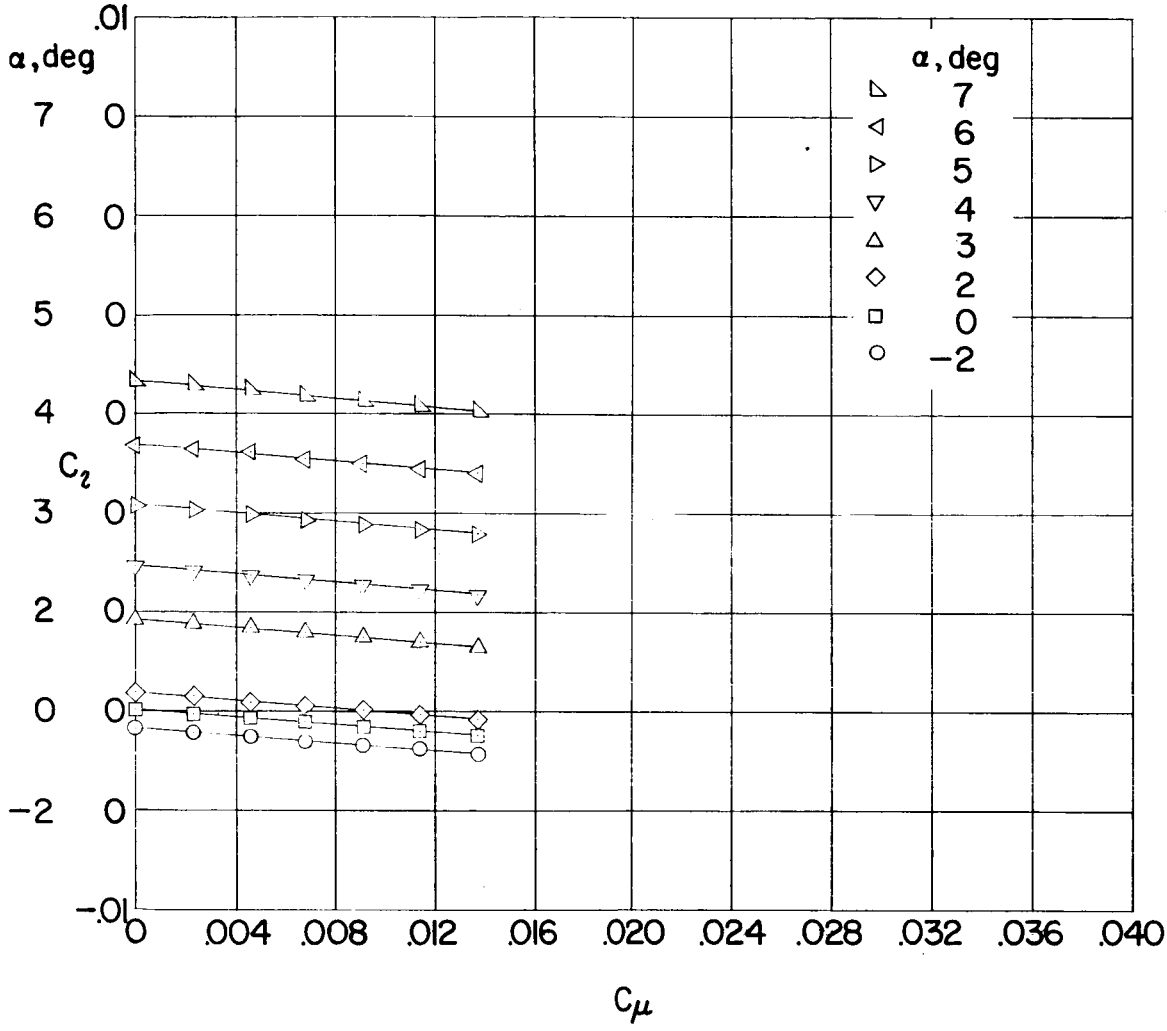

(f) Configuration 5; R = 2.8×10^6.

Figure 6.- Concluded.

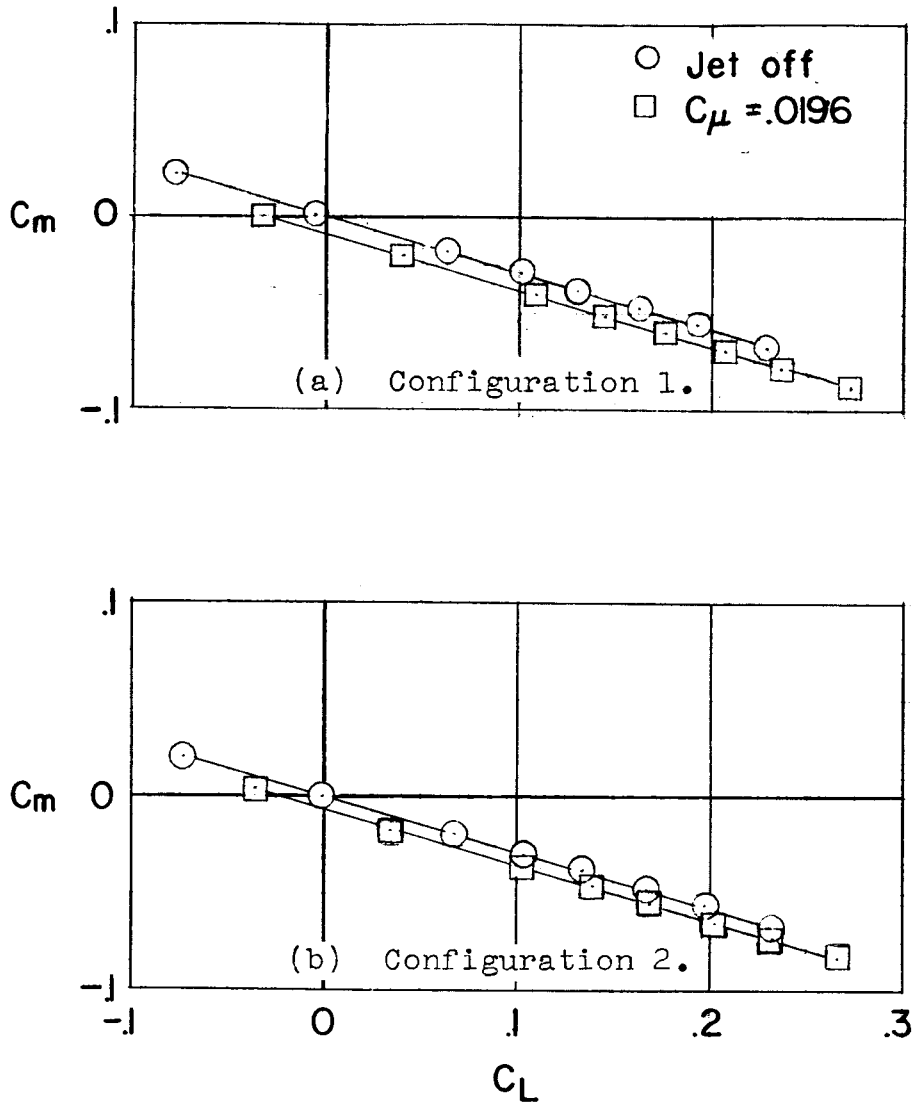

Figure 7.- Variation of C_m with C_L. $R = 2.8 \times 10^6$.

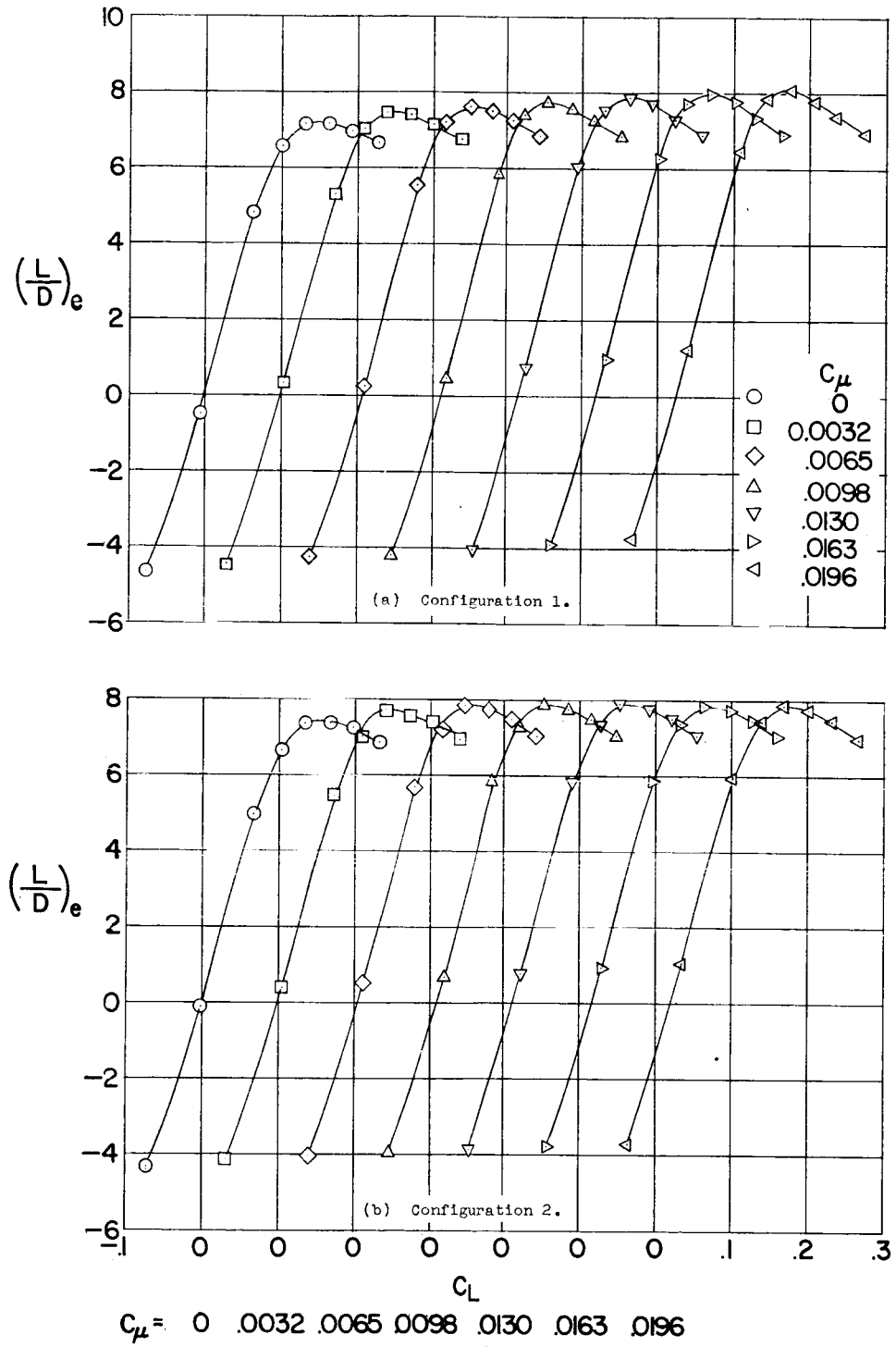

Figure 8.- Typical variation of $(L/D)_e$ with C_L. $R = 2.8 \times 10^6$.

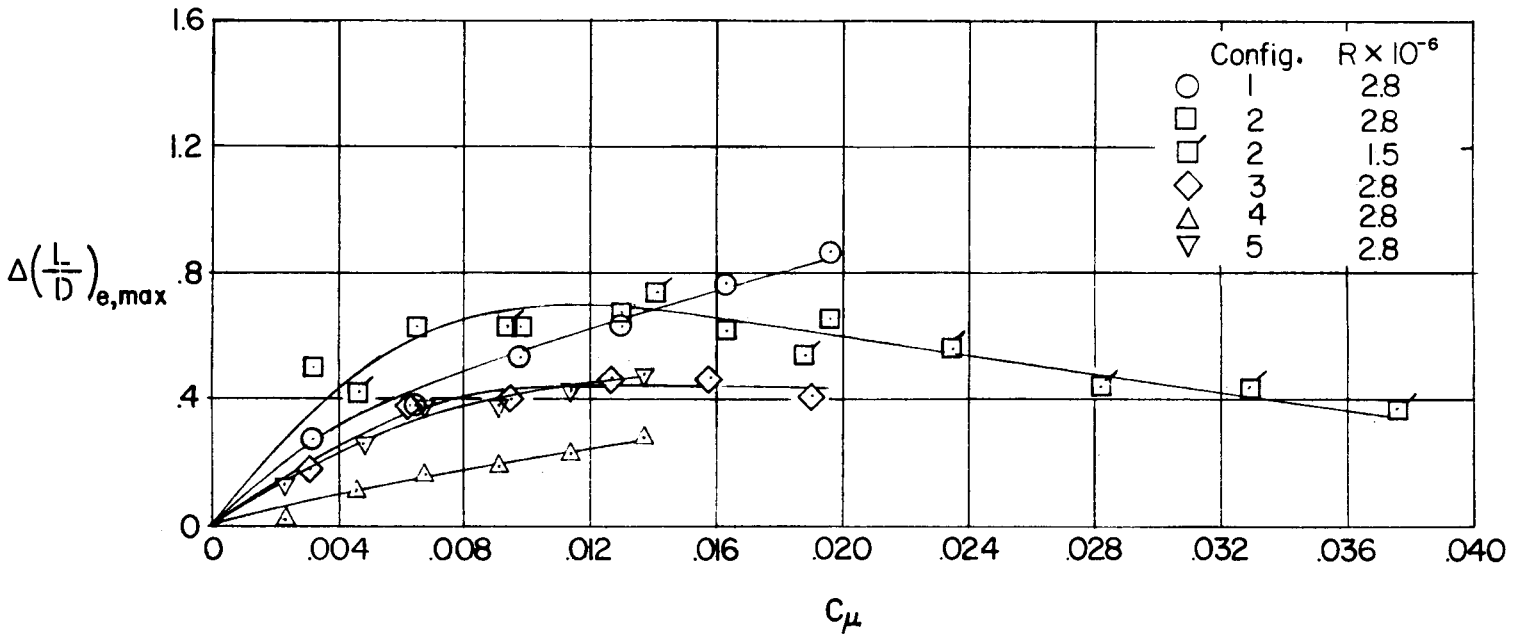

Figure 9.- Variation of $\Delta(L/D)_{e,max}$ due to jet with C_μ.

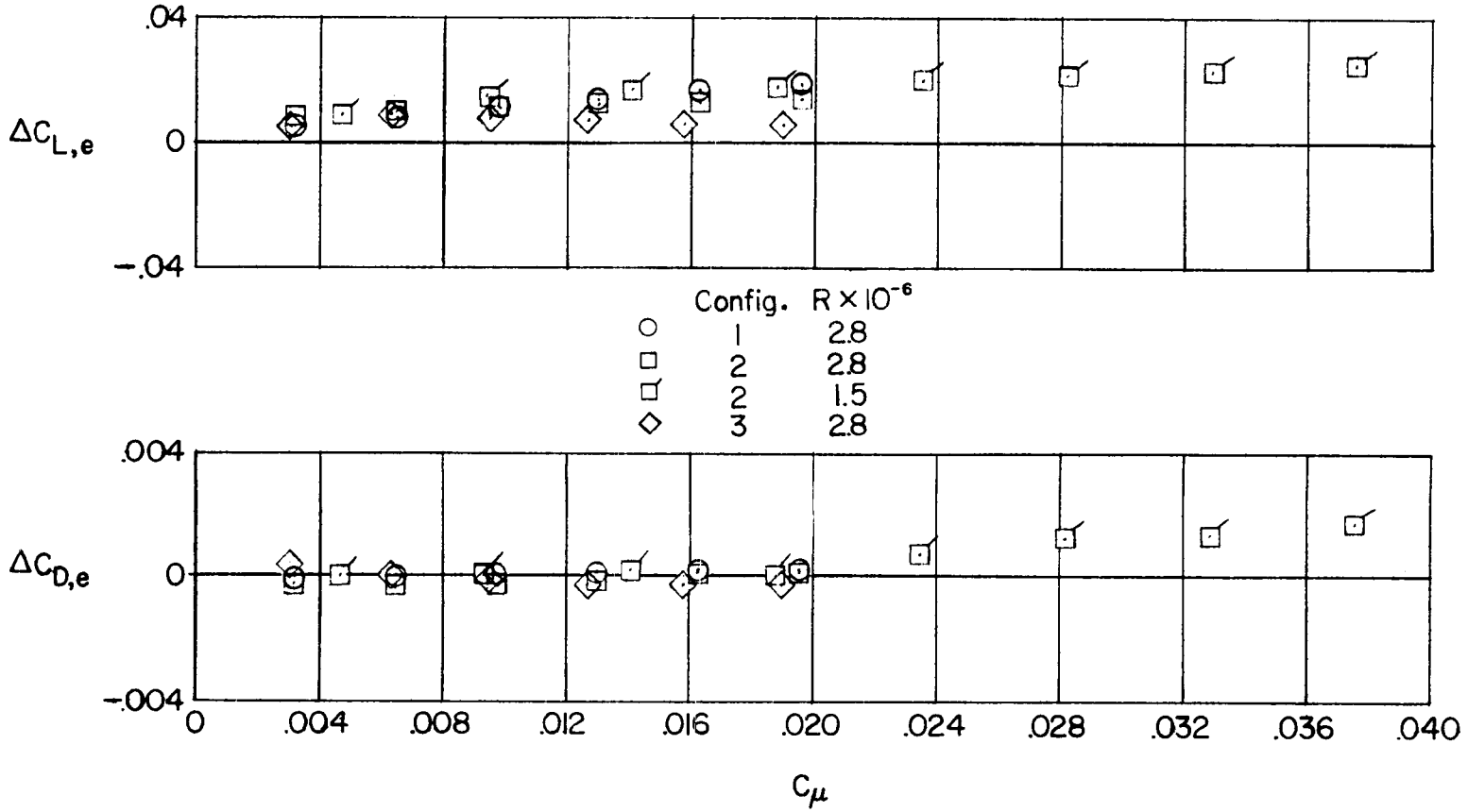

Figure 10.- Variation of incremental effective wing lift and drag coefficients with momentum coefficient. $\alpha = 4^\circ$ $\left(\text{near } (L/D)_{max}\right)$.

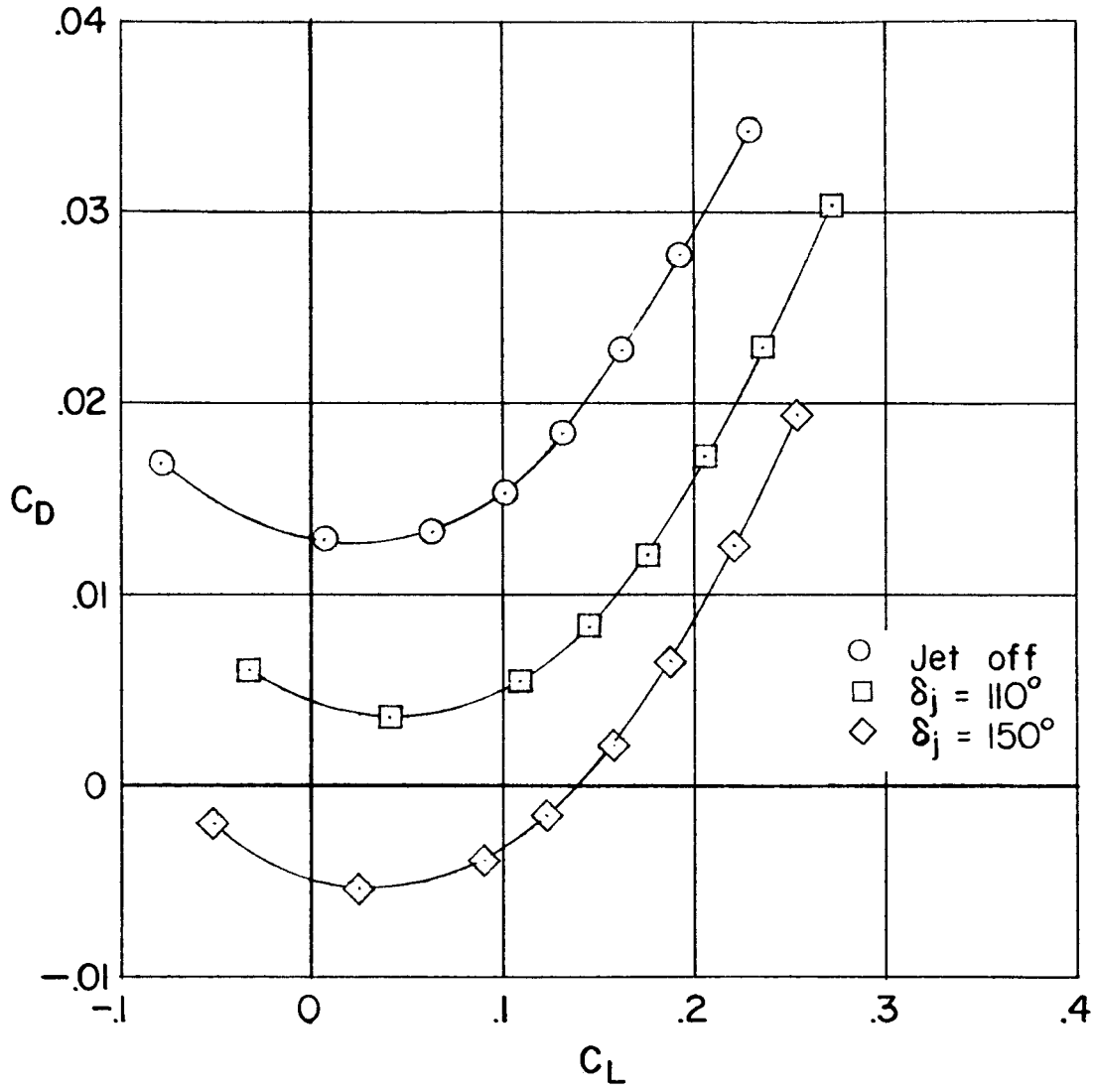

Figure 11.- Variation of C_D with C_L for jet-inoperative condition and for $\delta_j = 110°$ and $150°$ at $C_\mu \approx 0.020$. $R = 2.8 \times 10^6$.